applied sciences

MDPI

Article

Efficient and Sustainable Synthesis of Zinc Salt-Dependent Polycrystal Zinc Oxide Nanoparticles: Comprehensive Assessment of Physicochemical and Functional Properties

Johar Amin Ahmed Abdullah [1,*], Antonio Guerrero [1] and Alberto Romero [2,*]

[1] Departamento de Ingeniería Química, Escuela Politécnica Superior, Universidad de Sevilla, 41011 Sevilla, Spain; aguerrero@us.es
[2] Departamento de Ingeniería Química, Facultad de Química, Universidad de Sevilla, 41012 Sevilla, Spain
* Correspondence: jabdullah@us.es (J.A.A.A.); alromero@us.es (A.R.); Tel.: +34-954557179 (J.A.A.A. & A.R.)

Abstract: This research involved synthesizing zinc salt-dependent zinc oxide nanoparticles (ZS-ZnO-NPs) using different zinc salts ($ZnCl_2$, $ZnSO_4 \cdot H_2O$, $Zn(CH_3COO)_2 \cdot 2H_2O$, and $Zn(NO_3)_2 \cdot 6H_2O$) and plant extracts of *Phoenix dactylifera* L. The synthesis efficiency was evaluated, and to carry out further investigations, zeta potential measurements, as well as SEM and TEM examinations, were performed to assess the morphology and size distribution of the nanoparticles. XRD and UV-Vis spectroscopy were also employed to confirm the crystalline nature and optical properties of the synthesized ZS-ZnO-NPs, respectively. FTIR analysis was also performed to identify chemical groups on the nanoparticle surface. Furthermore, the ZS-ZnO-NPs' ability to scavenge free radicals ($FRs^{\bullet}$), and thus their antioxidant capacity, was assessed using the DPPH $FR^{\bullet}$ assay. The results showed that the type of zinc salt used for the synthesis significantly influenced the yield, stability, optical properties, morphology, and size distribution of nanoparticles. The zinc salt-dependent yield exhibited a notable range, varying from 50.3% to 55.3%. The nanoparticle size ranged from 3.7 to 10.2 nm, with the zeta potential ranging from −28.6 to −46.7 mV and the gap energy (E_g) ranging from 3.28 to 3.39 eV. Moreover, the synthesized ZS-ZnO-NPs exhibited concentration and time-dependent inhibitory activity against DPPH $FR^{\bullet}$, showing potential as antioxidant agents in biomedicine and other industries.

Keywords: zinc oxide nanoparticles; efficiency; stability; nanoparticle characterization; phytochemicals; zinc salts

Citation: Abdullah, J.A.A.; Guerrero, A.; Romero, A. Efficient and Sustainable Synthesis of Zinc Salt-Dependent Polycrystal Zinc Oxide Nanoparticles: Comprehensive Assessment of Physicochemical and Functional Properties. *Appl. Sci.* **2024**, *14*, 1815. https://doi.org/10.3390/app14051815

Academic Editors: Ivona Elez Garofulić and Maja Repajić

Received: 20 January 2024
Revised: 19 February 2024
Accepted: 20 February 2024
Published: 22 February 2024

1. Introduction

The ever-increasing demand for nanomaterials can be attributed to their remarkable properties that make them adaptable to a wide range of industries and applications. These cutting-edge materials have proven invaluable in diverse sectors, including but not limited to medical, chemical, pharmaceutical, mechanical, and several technological industries [1]. This field of research and development is widely regarded as one of the most prominent and pervasive topics across almost all academic disciplines [2]. Nanomaterials exhibit a variety of distinctive and unique properties, including exceptional chemical reactivity, remarkable strength, lightweight nature, enhanced surface exposure, and outstanding stability [3,4]. Zinc oxide nanoparticles (ZnO-NPs) have captured the attention of the scientific and medical communities due to their exceptional properties and versatility in applications [5]. ZnO-NPs are highly valuable materials with a multitude of properties that make them suitable for use in high-technology applications. The unique combination of exceptional chemical properties and excellent electrical, electronic, and physical properties has led to the widespread use of nanomaterials in a variety of fields. These properties include high photochemical stability, high electrochemical correlation coefficients, and the ability to act as optical detectors, light-emitting diodes, biological and chemical sensors, energy aggregators

such as electromagnetics, nano-molders, and solar cells [6]. Besides their applications in high-tech fields, ZnO-NPs have found important uses in cosmetics and drug delivery. Their ability to absorb UV radiation and act as antimicrobial agents make them valuable for treating various skin diseases. Additionally, ZnO-NPs are commonly used as an ingredient in medical products, such as sunscreens [7,8]. They possess inherent properties that make them effective in various fields, including high-tech industries, cosmetics, and medicine. These nanoparticles have gained wide usage in industrial and medical applications, having received approval from the FDA (Food and Drug Administration) in the United States for their safety and non-toxicity. Moreover, their unique ability to selectively target cancer and leukemic cells and bacteria has made them highly attractive in the field of drug delivery and gene delivery, biosensors, and cancer treatments [9–11]. Nanoparticles can be customized to combat specific diseases, making them particularly relevant in the field of medicine. They offer novel treatment options for diseases that are challenging to address due to size limitations [12].

Zinc oxide nanoparticles are a class of incredibly small particles with diameters of less than 100 nm. Depending on the manufacturing process used, these nanoparticles can possess a diverse range of chemical and physical properties. This flexibility makes them an exciting area of research, particularly in the field of medicine, where they hold great promise for developing innovative therapies that can target diseases previously thought to be untreatable due to their small size [13]. Several techniques have been developed to produce zinc oxide nanoparticles, including hydrothermal, sedimentation, sol-gel, and many others. Unfortunately, these methods are sometimes expensive and may require the use of hazardous chemicals, which poses a significant challenge in terms of sustainability and safety [14–17]. One recent trend in nanoparticle production has been the focus on more environmentally friendly and sustainable methods. As a result, many studies have explored the use of "green" techniques to produce noble metal nanoparticles. These methods aim to be simple, cost-effective, and easily repeatable, reducing the reliance on costly and potentially harmful chemical processes [18]. The significance of utilizing green technologies in nanoparticle production lies in their cost-effectiveness, non-toxicity, and ability to generate highly crystalline nanoparticles in various shapes and sizes. These environmentally friendly technologies often use plant or fruit extracts that contain polyphenols with unique properties. These polyphenols can reduce metal salts to create high-purity nanoparticles due to their characteristics, such as reducing abilities, hydrogen bonding, nucleophilicity, acidity, polarizability, and chelating capacity [19–21]. These exceptional properties have made nanoparticles a valuable resource for biomedical applications due to their high biocompatibility. Their production has increased significantly as a result of their numerous applications in the biomedical field [22–24].

Phoenix dactylifera L. is a versatile tree that offers a variety of benefits to humans, including food, medicine, fuel, and construction materials. This makes it known as the "Tree of Life". It has a broad range of medicinal, nutritional, and economic uses, including antimicrobials, food additives, anti-diabetes, and anti-lipidemic drugs. Researchers have discovered high levels of phytochemicals in this plant species, including polyphenols, flavonoids, terpenoids, aldehydes, alkaloids, fatty acids, etc. In addition, a range of metal oxide nanoparticles (MO-NPs), such as iron, gold, silver, and nickel oxide nanoparticles, have been created using this plant species. This highlights the importance of the phenolic compounds of *Phoenix* in various fields, including medicine and materials science [19,25–29]. *Phoenix dactylifera* L. materials offer potential pharmaceutical, biomedical, and food protection applications. They can be used as agents for anticancer, antibiotics, and antioxidant treatments. In addition, they can stabilize emulsions and be used in paints, membranes, and water and fertilizer treatment [30–36].

This study introduces a novel approach to synthesizing zinc salt-dependent zinc oxide nanoparticles (ZS-ZnO-NPs) by employing various zinc salts and a polyphenol-rich extract from *Phoenix dactylifera* L. We systematically explore the influence of different zinc salts on crucial nanoparticle characteristics, such as morphology, size distribution, crystalline

nature, optical properties, and surface chemical groups. This optimization process provides valuable insights into tailoring the green synthesis of ZS-ZnO-NPs for specific attributes. The evaluation of antioxidant capacity through the DPPH free radical assay underscores the potential applications of these environmentally friendly nanoparticles in biomedicine and industries, emphasizing the innovative contributions of this research to the field.

2. Materials and Methods

2.1. Materials

Zinc chloride anhydrous ($ZnCl_2$) was acquired from Sigma Aldrich (Merck KGaA, Darmstadt, Germany), zinc sulfate monohydrate ($ZnSO_4 \cdot H_2O$) was purchased from AppliChem GmbH (Darmstadt, Germany), zinc acetate dihydrate ($Zn(CH_3COO)_2 \cdot 2H_2O$) was acquired from Sigma Aldrich (Merck KGaA, Darmstadt, Germany), zinc nitrate hexahydrate ($Zn(NO_3)_2 \cdot 6H_2O$) was purchased from Lab-Honeywell (Wunstorfer Strasse, Seelze, Germany), and sodium hydroxide (NaOH) was purchased from PANEAC QUIMCA SAU (Barcelona, Madrid, Spain). DPPH (2,2-diphenyl-1-picrylhydrazyl) was obtained from Sigma Aldrich (Darmstadt, Germany). All other reagents and chemicals used in this study were of analytical quality.

Phoenix dactylifera L. extract was obtained as a modification of the method described in [26,37]. In brief, 5% (*w*/*v*) of *Phoenix* powder was mixed with water at 60 °C for 1 h. The extract was obtained by filtering the mixture through a cheesecloth.

2.2. Zinc Oxide Nanoparticle Preparation

The method used for the green synthesis of zinc salt-dependent ZnO-NPs (ZS-ZnO-NPs) was adapted from previous studies [38,39] with modifications to specifically focus on the use of an extract from *Phoenix dactylifera* L. that is rich in phytochemicals and acts as reducing and stabilizing agents, while also exploring the impact of different metal salts and molar masses on nanoparticle synthesis.

To start the synthesis, 0.1 M of various metallic salts of zinc, including $ZnCl_2$, $ZnSO_4 \cdot H_2O$, $Zn(CH_3COO)_2 \cdot 2H_2O$, and $Zn(NO_3)_2 \cdot 6H_2O$, were each dissolved in 20 mL of the extract. The resultant solution underwent pH adjustment to reach approximately 12, employing 5 M NaOH with the assistance of a pH meter [4,40]. This alkaline pH condition, facilitated by NaOH, serves a dual purpose in our synthesis process. Firstly, it overcomes the yield limitations commonly associated with the green synthesis of nanoparticles. Secondly, we have demonstrated in previous studies that nanoparticle formation is favored in a high pH medium, and NaOH acts as a critical agent in achieving and maintaining this optimal pH environment [4,40]. Subsequently, a theoretical calculation was conducted using Equation (1):

$$V_2 = \frac{V_1 C_1 (pH_{final} - pH_{initial})}{C_2} \quad (1)$$

This equation facilitated the determination of the required volume V_2 and concentration C_2 of the base for achieving the desired pH adjustment. In this context, V_1 and C_1 denote the volume and concentration of the precursor salt used in the reaction, while $pH_{initial}$ and pH_{final} represent the initial pH of the reaction and the target pH, respectively.

The reaction was stirred using a magnetic stirrer at a temperature of approximately 50 °C for 2–3 h until a green-colored precipitate formed. The precipitate was then filtered using Whatman No. 4 and meticulously rinsed with distilled water (DW) to eliminate any remaining suspended impurities. The pre-treatment of ZS-ZnO-NPs involved heating them at 100 °C for 8 h, followed by a final calcination treatment at 300 °C for 2 h. This concluding treatment facilitated the combustion of organic substances and the removal of impurities [37,41].

Efficiency of the Process

To evaluate the efficiency of the green synthesis method, the stoichiometry of the ZS-ZnO-NP formation was taken into account in the presence of polyphenolic compounds,

based on an earlier study, where the zinc salt (Zn X_2) was used as the limiting reactant (LR) [42]:

$$n\mathrm{ZnX_2} + 2n\mathrm{R\text{-}OH} \rightarrow n\mathrm{ZnO} + \mathrm{H_2O} + 2n\mathrm{R\text{-}X} \quad (2)$$

The efficiency % was obtained as follows:

$$\text{Efficiency } (\%) = \left(\frac{\text{mol ZnO produced}}{\text{mol ZnX}_2 \text{ feed}}\right) \times 100 \quad (3)$$

2.3. ZnO-NPs Characterization

2.3.1. Zetasizer Nano (Zeta Potentials Measurements)

To assess the zeta potential of the prepared ZS-ZnO-NPs, they were first dispersed in distilled water (4 mg/mL) and sonicated for 15 min before measurements. Next, approximately 900 µL of the dispersion was injected into DTS1070 cells, and measurements of zeta potential were performed using the Malvern Zetasizer Nano (ZSP, Malvern, UK) at a temperature of 25 °C. The obtained data were analyzed using Zetasizer Software 8.02 and labeled using OriginLab Pro 2019 for further analysis.

2.3.2. Scanning Electron Microscopy (SEM)

SEM was used as a characterization technique to determine the average diameter distributions and morphology of ZS-ZnO-NPs. First, the ZS-ZnO-NPs were dispersed in an ethanol solvent and sonicated for 30 min to ensure proper distribution. A small drop of the dispersion (≈2 µL) was then deposited onto an SEM stub using a conductive adhesive and allowed to dry completely. The sample was then scanned at various magnifications using a scanning electron microscope (Zeiss Auriga ZA, Wilson, NC, USA) operated at 30 kV acceleration voltage. The obtained images were used to analyze the size and shape of the different ZS-ZnO-NPs, as well as to compare the samples at different magnifications. Additionally, Image-J software (v1.53q, NIH, Bethesda, MD, USA) was utilized for elemental information labeling of the ZS-ZnO-NPs [43].

2.3.3. Transmission Electron Microscopy (TEM)

TEM was utilized as a characterization technique to ascertain the size and crystalline properties of the different ZS-ZnO-NPs. To prepare nanoparticles for TEM measurements, the ZS-ZnO-NPs were first dispersed in ethanol dispersant solvent, sonicated for 30 min to ensure the proper distribution of the nanoparticles, and then a small drop of the dispersion (≈2 µL) was placed onto a carbon-coated copper grid (CCCu grid) and left to dry completely. The CCCu grid was loaded onto a Talos S200 microscope (FEI, Hillsboro, OR, USA) and examined at an acceleration voltage of 200 kV under the electron beam to obtain high-resolution images of the nanoparticles and analyze their crystal structure. The elemental information labeling and the FFT function (Fast Fourier Transform) of ZS-ZnO-NPs were accomplished using Image-J, a widely used open-source image processing software in scientific research [43,44]. This software provided valuable insights into the structure and content of the image.

2.3.4. X-ray Diffraction (XRD)

The presence of crystalline phases in the sample was confirmed by obtaining an XRD pattern using a Brand diffractometer (Bruker Model D8 advance A25) equipped with Cu anode. The Debye–Scherrer formula, as outlined in earlier studies [26,45], was utilized to calculate the crystalline size of ZS-ZnO-NPs and their crystallinity degree. The diffractograms were generated within the range of 2θ (°) = 15–70.

2.3.5. Fourier Transform Infrared Spectroscopy (FTIR)

To gain insight into the structure of ZS-ZnO-NPs, the FTIR spectrometer (Hyperion 100 Spectrometer, Bruker, CA, USA) was used to analyze the vibration modes of the bonds present in the ZS-ZnO-NPs. This analysis was carried out over a general range of

4000–400 cm^{-1}. The spectrometer used a DTGS-KBr sensor configured in transmittance mode. Specific absorbance bands associated with the molecular structures of the ZS-ZnO-NPs were observed in three distinct areas at the global scale during the analysis. The first zone ranged from 3000 to 1800 cm^{-1} and contained the absorbance bands alkyl chains present on the surface of the NPs. The second zone, which ranged from 1800 to 900 cm^{-1}, contained the COO- band in oleates. The third and final zone ranged from 800 to 400 cm^{-1} and contained the Zn-O bonds in ZS-ZnO-NPs [46].

2.3.6. UV-Visible Absorption Spectra (UV-Visible)

The UV-visible absorption spectra were utilized to confirm the formation of ZS-ZnO-NPs and determine their gap energies by using a UV-spectrophotometer (Varian Cary 6000i, Santa Clara, CA, USA). This type of analysis provides an indirect measurement of absorbance and enables the calculation of the optical gap energy (Eg, eV) of the samples [26]. The Eg was figured out by Tauc's relation $\alpha = (B(h\upsilon - Eg)^n)/h\upsilon$, where α represents the dimensionless absorption coefficient computed from the absorbance A, $\alpha = (2.3023 \cdot A\ cm^{-1})$. The transition nature depends on the value of n, which takes 2 and $\frac{1}{2}$ for indirect and direct allowed transition, respectively, and 3 and 3/2 for indirect and direct forbidden transition, respectively. Additionally, h, υ, and B are Planck's constant, the frequency, and a material-dependent constant whose dimensions depend on the value of n (B = 1), respectively [47].

2.3.7. Antioxidant Activity (DPPH FR$^{\bullet}$ Assay)

The ability of the green-synthesized ZS-ZnO-NPs to scavenge free radicals (FRs$^{\bullet}$), which reflects their antioxidant capacity, was evaluated by measuring their response to DPPH radicals using the method outlined by [26]. To gain a comprehensive understanding of this property, the ZS-ZnO-NPs were tested at varying concentrations (50–1000 µg/mL) and incubation times (0.5–24 h). For each experiment, 2 mL of ZS-ZnO-NPs/DMSO solution dispersed in different concentrations was mixed with an equal volume of DPPH solution (7 mg/100 mL methanol). The mixtures were then incubated for 0.5, 3, 6, 12, and 24 h, and the absorbance at 517 nm was measured. To serve as a control, a mixture of DPPH/DMSO was prepared. The inhibition percentage (IP%) of the tested ZS-ZnO-NPs was calculated using the following formula: $IP\% = ((A_d - A_{da})/A_d) \times 100$. In this equation, A_d represents the absorbance value of the oxidized solution in the absence of ZS-ZnO-NPs antioxidant agent, while A_{da} represents the absorbance value after adding ZS-ZnO-NPs antioxidant agent.

2.3.8. Statistical Analysis

The samples underwent three measurements, and IBM SPSS software (Released 2019. IBM SPSS Statistics for Windows, IBM Corp, Armonk, NY, USA. Version 26.0) was used to conduct statistical analyses, reported as M ± SD. One-way ANOVA revealed significant differences at a 95% confidence level. Duncan's statistical analysis, a function applicable in one-way ANOVA, confirmed these significance levels ($p < 0.05$) while also assessing variance heterogeneity.

3. Results and Discussions

3.1. Process Efficiency

Efficiency is an important parameter to consider when synthesizing nanoparticles (NPs) since it indicates the molar number of NPs successfully synthesized. In this case, ZS-ZnO-NPs were synthesized using different zinc salts as precursors in *Phoenix dactylifera* L. extract, where the efficiency ranged from 48.0% to 55.3% (Figure 1).

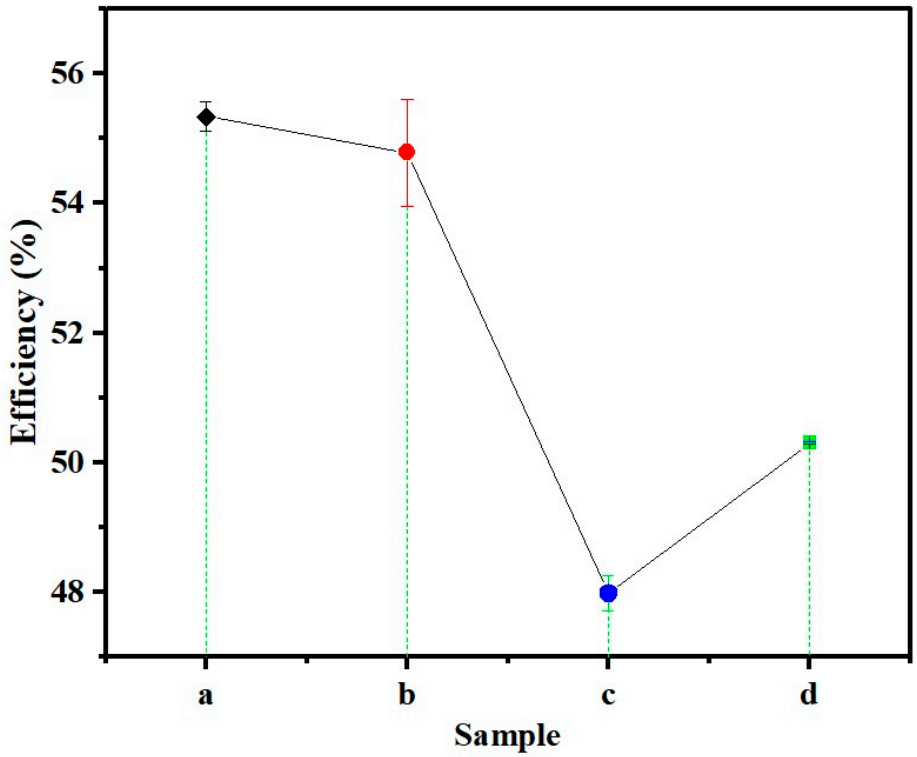

Figure 1. Process efficiency (%) of ZS-ZnO-NPs synthesis using different zinc salts and a plant extract of *Phoenix dactylifera* L. at pH 12: (a). $ZnCl_2$, (b). $ZnSO_4 \cdot H_2O$, (c). $Zn(CH_3COO)_2 \cdot 2H_2O$, and (d). $Zn(NO_3)_2 \cdot 6H_2O$.

Zinc chloride ($ZnCl_2$) and zinc sulfate ($ZnSO_4 \cdot H_2O$) showed the highest efficiencies, with no significant difference between them. On the other hand, zinc acetate ($Zn(CH_3COO)_2 \cdot 2H_2O$) exhibited the lowest efficiency at 48.0 ± 0.3%, and zinc nitrate ($Zn(NO_3)_2 \cdot 6H_2O$) had an intermediate efficiency of 50.3 ± 0.0% (Table 1).

Table 1. Results of efficiency (%), zeta potential (mV), diameter distribution average (nm) from TEM and SEM (D_{TEM} and D_{SEM}, respectively), and rod length (nm) for ZS-ZnO-NPs synthesized using different zinc salts and a plant extract of *Phoenix dactylifera* L. at pH 12: (a). $ZnCl_2$, (b). $ZnSO_4 \cdot H_2O$, (c). $Zn(CH_3COO)_2 \cdot 2H_2O$, and (d). $Zn(NO_3)_2 \cdot 6H_2O$.

	Sample	Efficiency (%)	Zeta Potential (mV)	D_{TEM}	D_{SEM}	Rod Length (nm)$_{SEM}$
a	$ZnCl_2$	55.3 ± 0.2^{A}	-46.7 ± 0.5^{A}	3.7 ± 0.2^{D}	6.4 ± 1.7^{D}	421.7 ± 184.2^{C}
b	$ZnSO_4 \cdot H_2O$	54.8 ± 0.8^{AB}	-28.6 ± 0.9^{D}	6.6 ± 0.1^{C}	9.4 ± 2.4^{C}	473.7 ± 184.8^{BC}
c	$Zn(CH_3COO)_2 \cdot 2H_2O$	48.0 ± 0.3^{D}	-32.5 ± 1.0^{C}	8.7 ± 0.3^{B}	14.7 ± 2.5^{B}	593.5 ± 230.2^{AB}
d	$Zn(NO_3)_2 \cdot 6H_2O$	50.3 ± 0.0^{C}	-41.5 ± 0.1^{B}	10.2 ± 0.3^{A}	19.6 ± 2.5^{A}	707.7 ± 307.2^{A}

Note: "±" indicates the standard deviation, and lowercase letters ($^{A–D}$) denote significant differences between samples based on statistical analysis.

The physicochemical properties of the zinc salts used can affect the formation, size, surface charge, and morphology of NPs, leading to variations in efficiency. For instance, the highly soluble zinc chloride (4320 g/L of H_2O at 25 °C [48]) may have contributed to the high efficiency of ZnO-NP synthesis by promoting rapid nucleation and crystal growth. In contrast, zinc acetate (40 g/L of H_2O at 25 °C [49]) has lower solubility, which may have resulted in a slower reaction rate and lower efficiency. Zinc sulfate (965 g/L of H_2O at room temperature [50]) and zinc nitrate have (1843 g/L of H_2O at 20 °C) intermediate solubilities and may have contributed to the observed intermediate efficiency values for the latter case.

The observed difference in efficiency between $ZnSO_4 \cdot H_2O$ and $Zn(NO_3)_2 \cdot 6H_2O$ prompts a closer examination of the influence of solubility on nanoparticle synthesis. While solubility is a critical factor, its impact is multifaceted. The highly soluble nature of zinc chloride likely contributed to the efficient synthesis of ZnO-NPs by promoting rapid nucleation and crystal growth. In contrast, despite the higher solubility of $Zn(NO_3)_2 \cdot 6H_2O$, other factors such as reaction kinetics and nucleation rate may have tempered its efficiency. It is crucial to acknowledge that solubility plays a pivotal role in shaping the synthesis process but interacts intricately with other kinetic and thermodynamic factors, which need to be assessed in future studies. The intermediate efficiency observed with zinc sulfate aligns with its moderate solubility, reinforcing the significance of solubility in the efficiency of nanoparticle synthesis. Nevertheless, these efficiency values fall within the reported range of green efficiency for synthesizing NPs using plant extracts, typically between 40 and 80% [51]. The reported efficiency of the ZnO-NPs synthesized in this study using different zinc salts remains lower than that of conventional synthesis methods, which can yield more than 90% efficiency. However, the specific mechanisms underlying the observed differences in efficiency between the different zinc salts require further investigation, as factors such as reaction conditions and pre- and post-treatment periods can affect the efficiency of conventional synthesis.

In addition to efficiency, the properties of the synthesized ZS-ZnO-NPs, including their size, shape, and functionality, should also be considered since they can affect the sustainability and potential applications of these materials. To this end, Zeta potential, XRD, SEM, and TEM were used to study the size and morphology of the ZS-ZnO-NPs synthesized in this work.

3.2. Zeta Potential

The zeta potential is a measure of the electrostatic potential difference between the dispersion medium and the surface of the particles. It is an important parameter that can affect the stability of the NPs in the dispersion medium. A higher absolute value of the zeta potential indicates greater stability of the NPs in the medium. In this investigation, we observed differences in the zeta potential values of the green-synthesized ZS-ZnO-NPs, which could be attributed to the different types of zinc salts used as precursors. The variation in the zeta potential of the ZS-ZnO-NPs synthesized using different zinc salts can be explained by the physicochemical properties of the zinc salts, which affect the formation, size, and morphology of the NPs. In this case, zinc chloride exhibited the highest zeta potential value at -46.7 ± 0.5 mV (Figure 2 (a)), followed by Zinc nitrate at -41.5 ± 0.1 mV (Figure 2 (d)). Zinc sulfate ($ZnSO_4 \cdot H_2O$) showed the lowest zeta potential value at -28.6 ± 0.9 mV (Figure 2 (b)), while Zinc acetate had an intermediate value at -32.5 ± 1.0 mV (Figure 2 (c)).

The differences in the zeta potential values could be attributed to the different surface charges of the synthesized nanoparticles, which are influenced by several factors, including size, shape, and surface functionalization. The type of precursor used may have affected the size, structure, and shape of these nanoparticles, which could explain the observed differences in the zeta potential values [52]. The results suggest that the type of zinc salt precursor used can significantly influence the zeta potential of the synthesized ZS-ZnO-NPs, which may be attributed to the solubility and surface charge of the zinc salts. Further investigation using TEM and SEM techniques was conducted to understand the specific characteristics underlying these differences.

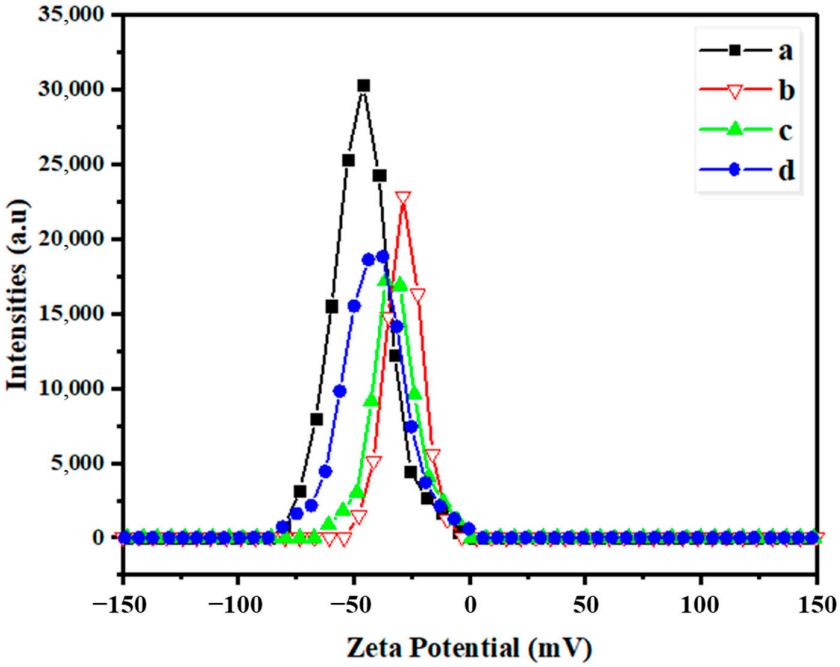

Figure 2. Zeta potential values of ZS-ZnO-NPs synthesized using different zinc salts and a plant extract of *Phoenix dactylifera* L. at pH 12: (a). $ZnCl_2$, (b). $ZnSO_4 \cdot H_2O$, (c). $Zn(CH_3COO)_2 \cdot 2H_2O$, and (d). $Zn(NO_3)_2 \cdot 6H_2O$.

3.3. SEM

The morphology of ZS-ZnO-NPs synthesized using different zinc salts was investigated using a green synthesis method under the same conditions, and SEM characterization was performed to determine their shape and size. The results showed that the type of zinc salt used significantly affected the morphology of the nanoparticles. As shown in Figure 3, SEM characterization revealed that ZS-ZnO-NPs synthesized using $ZnCl_2$ exhibited a unique mixture of random, conglomerated, packed, clustered, and rod-shaped NPs with face-centered rhombohedral, spherical, hexagonal, and cubic-like structures.

$ZnSO_4 \cdot H_2O$ resulted in the formation of nanorods, nanoplate flower-like nanolayered, and hollow spherical morphologies, while $Zn(CH_3COO)_2 \cdot 2H_2O$ promoted the formation of needle-shaped nanorods, thinner nanoplate, and flower-like nanolayered morphology. In contrast, $Zn(NO_3)_2 \cdot 6H_2O$ led to the formation of larger nanorods, flower-like, nanolayered, and some cubic structures. Previous literature has reported similar morphologies [20,53]. The diameter distribution and rod length (grain size) of the ZS-ZnO-NPs varied depending on the type of zinc salt used, as summarized in Table 1. The size distribution of the ZS-ZnO-NPs followed the order of $ZnCl_2 < ZnSO_4 \cdot H_2O < Zn(CH_3COO)_2 \cdot 2H_2O < Zn(NO_3)_2 \cdot 6H_2O$, with distribution diameter average ranging from 6.4 ± 1.7 to 19.6 ± 2.5 nm (Figure 3).

The use of different zinc salts resulted in differences in the size and morphology of the green-synthesized ZS-ZnO-NPs. The anions used can affect nanoparticle stability and aggregation, and the Hofmeister series can be used to predict their effectiveness. Sulfate (SO_4) and chloride (Cl_2) ions are more effective in reducing aggregation and stabilizing the surface charge, while carboxylate (COOH) and nitrate (NO_3) ions tend to promote aggregation and result in larger nanoparticles. Therefore, the smaller size of the nanoparticles synthesized using $ZnSO_4 \cdot H_2O$ and $ZnCl_2$ compared to $Zn(CH_3COO)_2 \cdot 2H_2O$ and $Zn(NO_3)_2 \cdot 6H_2O$ could be due to the higher effectiveness of sulfate and chloride ions in reducing aggregation and stabilizing the surface charge. On the other hand, the smaller size of the ZnO-NPs synthesized using $Zn(CH_3COO)_2 \cdot 2H_2O$ compared to $Zn(NO_3)_2 \cdot 6H_2O$ could be due to the lower hydration of carboxylate ions compared to nitrate ions [54]. The dissociation of nitrate ions is known to be more effective in solution due to their higher solubility and ability to form more hydrated species. In contrast, carboxylate ions exhibit

lower hydration tendencies. This difference in hydration levels may have influenced the nucleation and growth processes during synthesis, resulting in the smaller size observed in the ZnO-NPs synthesized using $Zn(CH_3COO)_2{\cdot}2H_2O$.

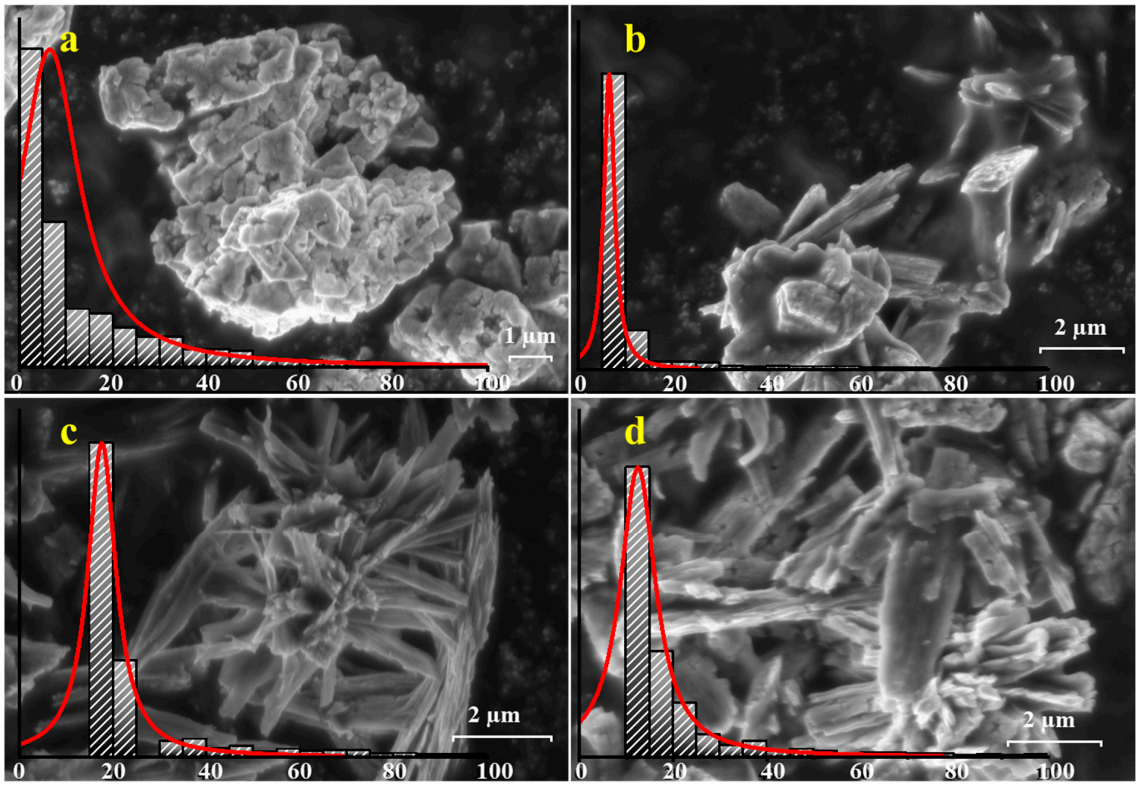

Figure 3. Scanning electron microscopy (SEM) of ZS-ZnO-NPs synthesized using different zinc salts and a plant extract of *Phoenix dactylifera* L. at pH 12: (**a**). $ZnCl_2$, (**b**). $ZnSO_4{\cdot}H_2O$, (**c**). $Zn(CH_3COO)_2{\cdot}2H_2O$, and (**d**). $Zn(NO_3)_2{\cdot}6H_2O$. Diameter distribution averages (in nm) were included, respectively.

However, it is crucial to note that the study referenced [54] obtained its results using reverse microemulsion systems and an acidic environment. Emphasis was placed on the use of ethanol as the washing solvent and drying at 30 °C in that study. In contrast, our work employed a green synthesis method utilizing *Phoenix dactylifera* L. extract in an alkaline environment, with nanoparticles washed using water. Although our results align with those of [54], recognizing the differences in experimental conditions is crucial. Investigating these parameters may contribute to understanding the behavior or reversal of the Hofmeister series, and a comprehensive investigation of factors such as pH and salt concentration is warranted. Furthermore, recent insights from a review [55] underscore the potential perturbation of specific ion effects (SIEs) by various stimuli, encompassing solvent, temperature, and UV radiation. This expands the traditional understanding of SIEs induced by factors like concentration, pH, cosolute, and counterion. Therefore, considering these broader factors can provide a more nuanced and comprehensive understanding of the complex interplay involved in nanoparticle synthesis and behavior.

The morphologies observed in the ZS-ZnO-NPs further demonstrate the influence of metal salts on nanoparticle morphology. The presence of phytochemicals in the extract acting as stabilizing agents, along with reflux conditions, may lead to agglomeration, while in some cases, slight agglomeration may result from nanoparticle interactions. Furthermore, nanoparticles can appear as agglomerates or aggregates due to the presence of bioactive molecules that form hydrogen bonds. These observations are consistent with the previous literature [56–59]. While SEM provided valuable insights into the nanoparticle morpholo-

gies, further TEM analysis would be needed to precisely determine the particle sizes and morphology, as well as to investigate the atomic structure and defects of the ZS-ZnO-NPs.

3.4. TEM

The effect of different zinc salts on the morphology (Figure 4) and size distribution of ZS-ZnO-NPs was investigated using a green synthesis method under the same conditions.

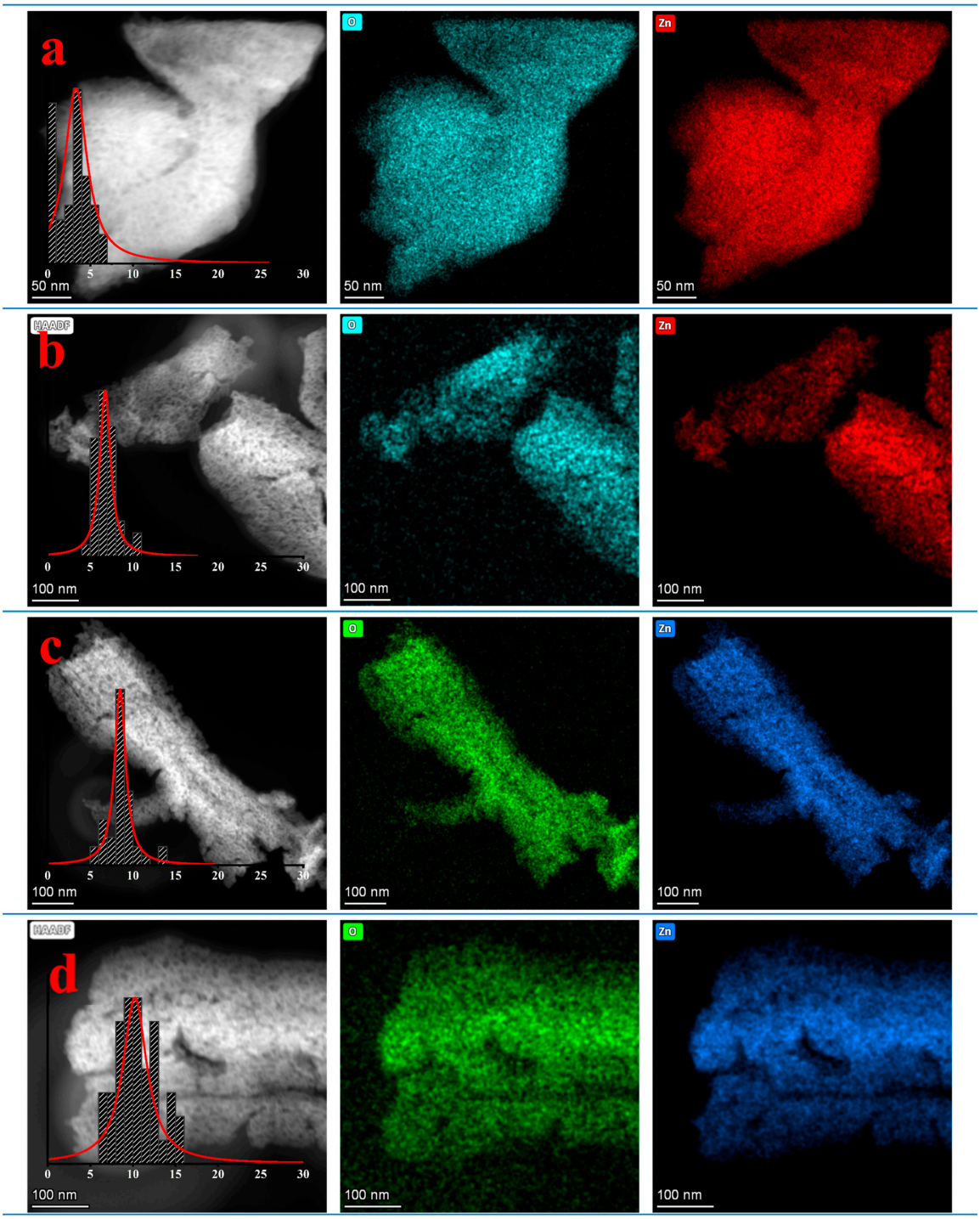

Figure 4. Transmission electron microscopy (TEM) and the respective elemental energy-dispersive X-ray spectroscopy (EDX) analysis of ZS-ZnO-NPs synthesized using different zinc salts and a plant extract of *Phoenix dactylifera* L. at pH 12: (**a**). $ZnCl_2$, (**b**). $ZnSO_4 \cdot H_2O$, (**c**). $Zn(CH_3COO)_2 \cdot 2H_2O$, and (**d**). $Zn(NO_3)_2 \cdot 6H_2O$. Diameter distribution from TEM images was included.

The nanoparticles exhibited diverse morphologies with weakly differentiated agglomeration in various shapes, which can be attributed to the flower-like behavior and elongation caused by the competition between the functional compounds and zinc-dependent ions on the particle's surface [20,53]. Elemental analysis using EDX revealed no presence of elements other than O-Zn in the samples (Figure 4). The diverse morphologies observed in ZS-ZnO-NPs, as determined by fast Fourier transform (FFT), can be attributed to the distinct influence of various zinc salts used during synthesis. In the case of $ZnCl_2$, the hexagonal-centered cub-like shapes with facets and star-shaped morphology may be linked to the smaller ionic radius of chloride ions (approximately 181 pm) [60], promoting strong electrostatic interactions and influencing nucleation and growth. $ZnSO_4 \cdot H_2O$ resulted in the formation of hollow spherical structures, nanorings, and spheroidal morphology, likely due to the larger ionic radius of sulfate ions (approximately 211 pm) [60], introducing steric hindrance and impacting nanoparticle arrangement. $Zn(CH_3COO)_2 \cdot 2H_2O$ promoted the formation of larger particles with faceted morphology and triclinic symmetry, with the variable ionic radius of acetate ions influencing growth processes. Lastly, $Zn(NO_3)_2 \cdot 6H_2O$ produced larger particles with a single crystal structure, possibly influenced by the ionic radius of nitrate ions (approximately 190 pm). This comprehensive understanding underscores the size-dependent effects of different anions on the resulting morphology of ZS-ZnO-NPs [61,62].

The size distribution of the ZS-ZnO-NPs followed the order of $ZnCl_2$ < $ZnSO_4 \cdot H_2O$ < $Zn(CH_3COO)_2 \cdot 2H_2O$ < $Zn(NO_3)_2 \cdot 6H_2O$, with very small particle sizes ranging from 3.7 to 10.2 nm (Figure 5). Similar morphologies have been reported in the previous literature [63–66]. The results suggest that the choice of zinc salt has a significant impact on the morphology and size distribution of ZS-ZnO-NPs, with some salts promoting the formation of small, well-defined nanoparticles, while others promote the formation of larger, more complex nanoparticles with a variety of crystal symmetries.

The TEM results agree with SEM regarding the effect of the metal salt on the particle size distribution, but the measurements are notably smaller than those obtained via SEM. The difference in particle size measurements between SEM and TEM can be attributed to different imaging techniques and sample preparation methods. Inconsistent calibration and variations in contrast production among microscopes can exaggerate particle size in SEM. In contrast, the sample preparation technique, such as smearing a dispersion droplet on an SEM stub using a conductive coating for SEM or applying a dispersion drop onto a holey carbon-coated copper for TEM, can lead to bias towards smaller sizes for TEM [67]. These factors can lead to discrepancies between the two techniques, making it essential to carefully evaluate and consider the results obtained by both methods.

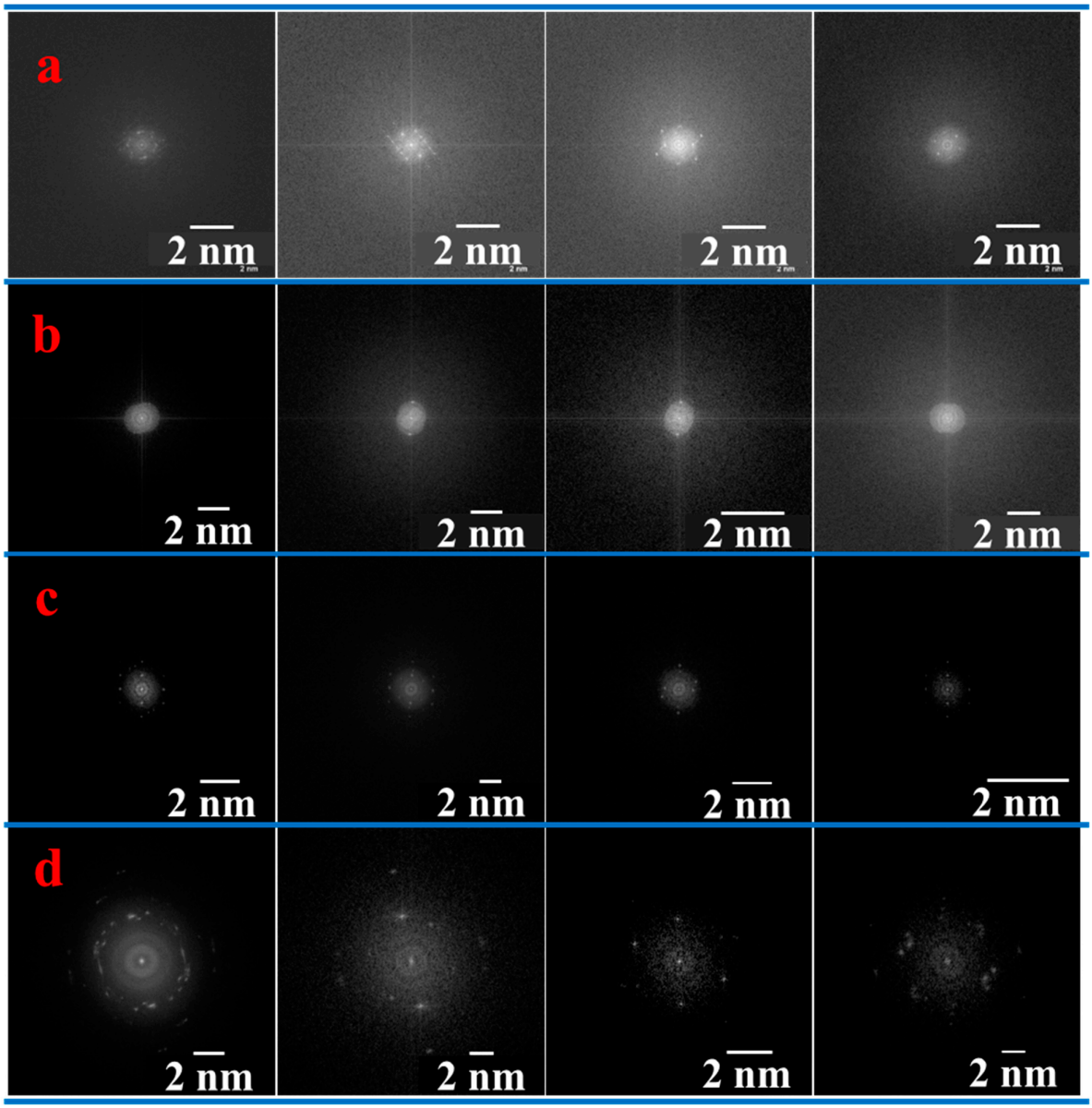

Figure 5. FFT illustrating the distinct crystalline structures of ZS-ZnO-NPs synthesized using different zinc salts and a plant extract of *Phoenix dactylifera* L. at pH 12: (**a**). $ZnCl_2$, (**b**). $ZnSO_4{\cdot}H_2O$, (**c**). $Zn(CH_3COO)_2{\cdot}2H_2O$, and (**d**). $Zn(NO_3)_2{\cdot}6H_2O$.

3.5. XRD

XRD was used to analyze the crystal structure of the ZS-ZnO-NPs synthesized using different zinc salts. Figure 6 shows the XRD patterns of the ZS-ZnO-NPs synthesized using different metal salts.

The diffraction peaks observed in all samples at 2θ (°) = 31.85, 34.46, 36.30, 47.59, 56.67, 62.89, 66.57, 68.1, and 69.10 were attributed to the crystallographic reflection's planes (100), (002), (101), (102), (110), (103), (200), (112), and (201), which corresponded to the characteristic peaks of the hexagonal wurtzite structure of ZnO (JCPDS n°.01-079-2205) [68], confirming the successful synthesis of ZS-ZnO-NPs. The peak intensity and position exhibited variations depending on the type of zinc salt employed, particularly at the most intense peak (101) for each ZnO-NPs spectrum. ZS-ZnO-NPs synthesized with $ZnCl_2$ demonstrated superior crystallinity, showing a degree of crystallinity of 28.1% in Figure 6a. In comparison, $ZnSO_4{\cdot}H_2O$, $Zn(CH_3COO)_2{\cdot}2H_2O$, and $Zn(NO_3)_2{\cdot}6H_2O$ resulted in lower crystallinities at the same peak, with values of 27.6% (Figure 6b), 27.1%

(Figure 6c), and 14.8% (Figure 6d), respectively. The variation in peak intensities is likely attributed to differences in zinc ion concentrations and the nature of anions in the various zinc salts, impacting the growth and nucleation of ZS-ZnO-NPs [63,69,70]. This observation aligns with studies on the prolongation of oxidation time, where a similar effect in peak intensity and corresponding crystallinity was noted. This phenomenon was explained by the preferential growth of ZnO nanostructures along the c-axis as wet oxidation progressed from 2 to 8 h [71,72]. When varying the anion, the application of the Hofmeister series can offer insights, as discussed in Section 3.3.

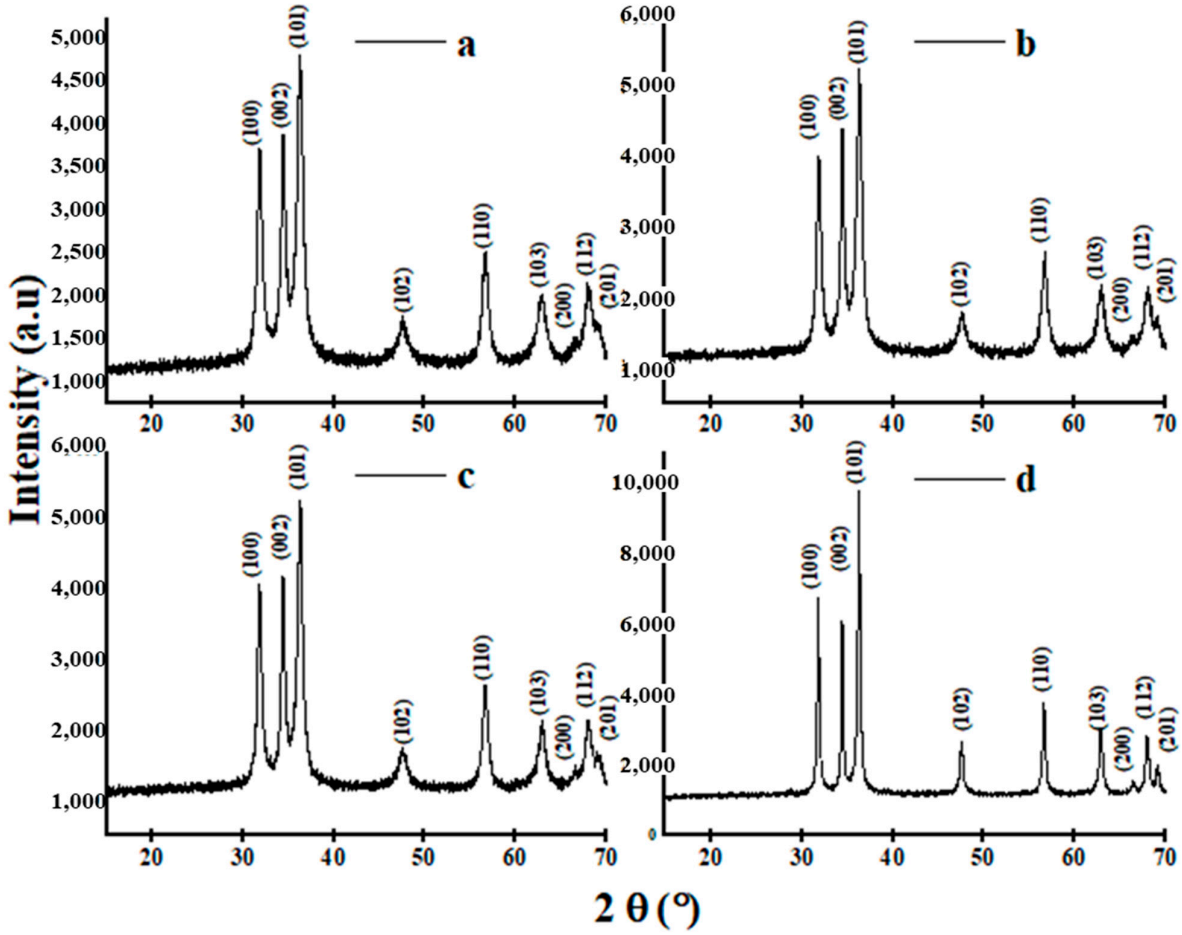

Figure 6. XRD spectra of ZS-ZnO-NPs synthesized using different zinc salts and a plant extract of *Phoenix dactylifera* L. at pH 12: (**a**). $ZnCl_2$, (**b**). $ZnSO_4 \cdot H_2O$, (**c**). $Zn(CH_3COO)_2 \cdot 2H_2O$, and (**d**). $Zn(NO_3)_2 \cdot 6H_2O$. Standard ZnO diffraction pattern; JCPDS n°.01-079-2205.

The synthesis mechanism for the formation of zinc oxide nanoparticles (ZnO-NPs) using various zinc salts ($ZnCl_2$, $ZnSO_4 \cdot H_2O$, $Zn(CH_3COO)_2 \cdot 2H_2O$, and $Zn(NO_3)_2 \cdot 6H_2O$) and *Phoenix dactylifera* L. extract involves a complex interplay of chemical reactions and molecular processes. The eco-friendly synthesis process is depicted in Figure 7, emphasizing the role of *Phoenix dactylifera* L. extract as a rich source of polyphenols, which act as non-toxic antioxidants facilitating the reduction of metal precursors to ZnO-NPs. The use of polyphenols contributes to green synthesis by stabilizing the nanoparticles without generating toxic by-products, aligning with environmentally sustainable practices [19,73,74].

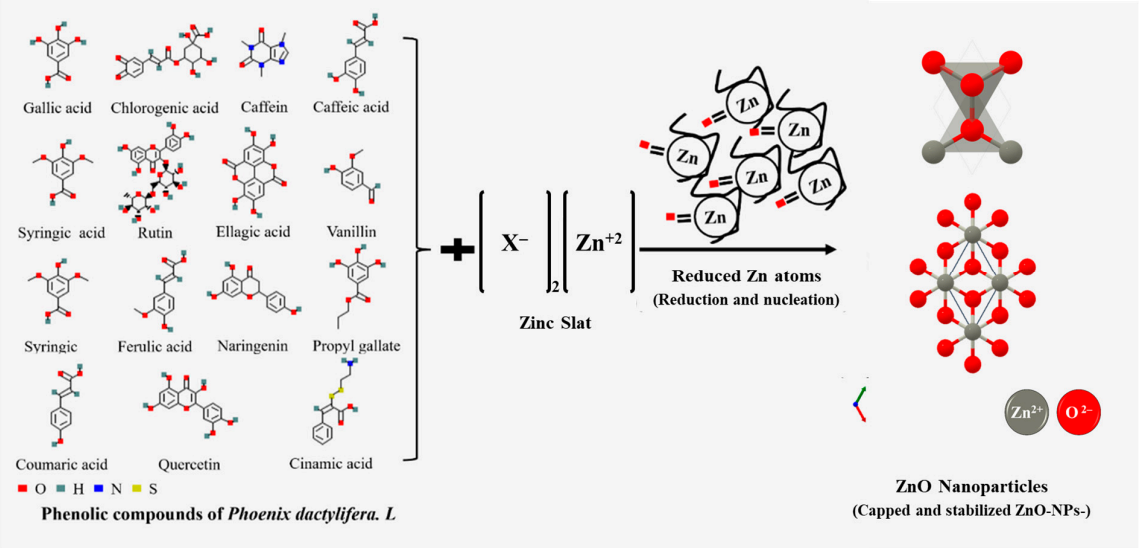

Figure 7. Growth mechanism for the sustainable synthesis of zinc salt-dependent hexagonal zinc oxide nanoparticles.

The synthesis process can be delineated into three key phases [29,75,76]:

1. Activation Phase: This initial phase involves precursor formation, metal ion reduction (neutralization reactions), and metal ion nucleation. The reduction of metal ions by phytochemicals, particularly polyphenols, plays a pivotal role in initiating the synthesis process.
2. Growth Phase: This phase is crucial for nanoparticle stability. The stabilized metal ions undergo further growth, contributing to the stability of the formed nanoparticles.
3. Termination Phase: In this phase, the shape of nanoparticles is determined. Aging processes, such as coarsening and aggregation, occur, influencing the final morphology of the nanoparticles.

Studies propose that metal ions, post-reduction by phytochemicals, may undergo coverage by organic compounds in these three phases for stabilization. The nucleation kinetics are closely associated with chemical reaction kinetics and molecular mechanisms. The growth mechanism of ZnO nanoparticles (ZnO-NPs) formation using various zinc salts, including $ZnSO_4 \cdot H_2O$, $Zn(CH_3COO)_2 \cdot 2H_2O$, and $Zn(NO_3)_2 \cdot 6H_2O$ and *Phoenix dactylifera* L. extract in water involves a chemical reaction described by Equation (4) [76]:

$$nZnX_2 + 2n\text{R-OH} + lH_2O \rightarrow {Zn^{2+}}_n(OH^-)_m(H_2O)_l{X^-}_k + (2n - k)X^- + (2n - m)\ OH^- + 2n\text{R}^+ \rightarrow n\text{ZnO} + (l + n)\ H_2O + 2n\text{R-X} \quad (4)$$

In this equation:

- ZnX_2 represents the zinc salt, where X is the anion (e.g., Cl^-, ${SO_4}^{2-}$, CH_3COO^-, ${NO_3}^-$).
- R-OH represents the phenolic compounds in the plant extract.
- H_2O is water.
- ${Zn^{2+}}_n(OH^-)_m(H_2O)_l{X^-}_k$ is the zinc-ligand molecule acting as a nucleation precursor.
- $(2n - m)\ OH^-$, and $2n\text{R}^+$ are byproducts.
- nZnO is the formed zinc oxide nanoparticles.

The selection of different zinc salts, each accompanied by a distinct anion (*X*), holds significant implications for the synthesis of zinc oxide nanoparticles (ZnO-NPs). The chemical reactivity of varied anions, such as chloride (Cl^-), sulfate (${SO_4}^{2-}$), acetate (CH_3COO^-), and nitrate (${NO_3}^-$), influences the nucleation kinetics during the synthesis process. The anion plays a pivotal role in forming precursors, impacting the stability and reactivity of zinc–ligand molecules. Solubility differences arising from the nature of the anion affect

supersaturation levels, influencing the timing and extent of nucleation. Furthermore, the anion's role in stabilizing the formed nanoparticles and its interactions with polyphenols from the plant extract contribute to variations in the growth and termination phases. Plant polyphenols cause metals to form their metal oxides and make them reach the growth and stabilization phases. Finally, by binding metal ions to oxygen, nanoparticles with a defined shape are formed at the final treatment with the annealing temperatures [29,75]. Hence, understanding the specific contributions of each anion is crucial for tailoring the synthesis method and achieving desired characteristics in the resulting ZnO-NPs, exemplifying the nuanced impact of anion choice on the overall nanoparticle synthesis process [76].

The crystallite size of the ZS-ZnO-NPs was estimated using the Debye–Scherrer equation [26,45]. Therefore, the average crystallite sizes of the ZS-ZnO-NPs were in the range of 9.3 ± 0.5 to 22.6 ± 1.4 nm (Table 2), which were consistent with the particle sizes determined by SEM, and TEM analysis. The XRD results definitively confirm the presence of ZnO-NPs, as evidenced by distinct peaks aligning with the hexagonal structure. This affirmation underscores the purity of the synthesized nanoparticles, as no supplementary peaks indicative of impurities were observed, consistent with TEM and EDX findings (refer to Section 3.4). Furthermore, we bolstered the comprehensive characterization of the nanoparticles by employing FTIR and UV-visible spectroscopy in the following sections. These additional techniques were utilized to not only validate the formation of ZnO-NPs but also to delve into their optical properties, specifically focusing on the band gap energy.

Table 2. Results of diameter average from XRD (Avg D_{XRD}, nm), diameter at the most intense peak ($D_{(101)}$, nm), $FWHM_{(101)}$, and crystallinity degree (%) for ZS-ZnO-NPs synthesized using different zinc salts and a plant extract of *Phoenix dactylifera* L. at pH 12: (a). $ZnCl_2$, (b). $ZnSO_4{\cdot}H_2O$, (c). $Zn(CH_3COO)_2{\cdot}2H_2O$, and (d). $Zn(NO_3)_2{\cdot}6H_2O$.

	Sample	Avg $D_{XRD(nm)}$	$D_{(101)}$	$FWHM_{(101)}$	Crystallinity (%)
a	$ZnCl_2$	9.3 ± 0.5^{D}	11.94^{D}	0.70^{A}	94.6^{A}
b	$ZnSO_4{\cdot}H_2O$	10.9 ± 0.7^{C}	12.29^{C}	0.68^{B}	93.3^{B}
c	$Zn(CH_3COO)_2{\cdot}2H_2O$	12.4 ± 0.7^{B}	13.06^{B}	0.64^{C}	92.5^{C}
d	$Zn(NO_3)_2{\cdot}6H_2O$	22.6 ± 1.4^{A}	25.33^{A}	0.33^{D}	83.5^{D}

Note: "±" indicates the standard deviation, and uppercase letters ($^{A–D}$) denote significant differences between samples based on statistical analysis.

$ZnCl_2$ resulted in the smallest crystallite size, while $Zn(NO_3)_2{\cdot}6H_2O$ produced the largest crystallite size. Consistent with previous studies, the results demonstrate the impact of zinc salt precursor on ZS-ZnO-NPs crystallite size [58,76]. The diverse morphologies observed in the SEM images are also reflected in the XRD patterns, as evidenced by the broadening of the diffraction peaks, which indicates a certain degree of structural disorder caused by the presence of different morphologies or crystallographic orientations of ZS-ZnO-NPs [76,77]. The XRD patterns show a slight broadening of the diffraction peaks, suggesting the presence of small nanoparticles, which may be due to the agglomeration of nanoparticles observed in the SEM images.

Overall, the XRD analysis confirmed the successful synthesis of ZS-ZnO-NPs using different zinc salts and showed that the crystallinity and crystallite size of the nanoparticles depended on the type of zinc salt used. The diverse morphologies observed in the SEM and TEM images were also reflected in the XRD diffractograms, indicating the presence of different crystallographic orientations of ZS-ZnO-NPs.

3.6. FTIR

FTIR analysis was conducted to investigate the functional and chemical groups present in the synthesized ZS-ZnO-NPs. Figure 8 shows the FTIR spectra of the ZS-ZnO-NPs synthesized using different zinc salts.

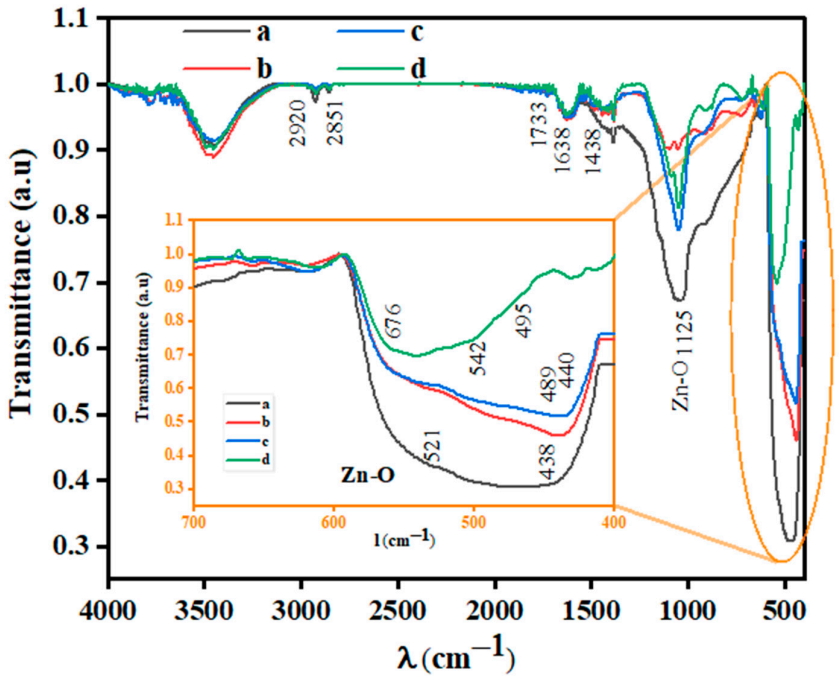

Figure 8. FTIR spectrum of the transmittance of ZS-ZnO-NPs synthesized using different zinc salts and a plant extract of *Phoenix dactylifera* L. at pH 12: (a). $ZnCl_2$, (b). $ZnSO_4 \cdot H_2O$, (c). $Zn(CH_3COO)_2 \cdot 2H_2O$, and (d). $Zn(NO_3)_2 \cdot 6H_2O$.

The observed peaks were assigned to various functional groups based on the literature [20,65]. All of the synthesized ZS-ZnO-NPs exhibited characteristic peaks in the range of 4000–400 cm^{-1}, indicating the stretching vibrations of O–H, which can be attributed to the presence of adsorbed water on the particle surface [78]. The peak between 3500 and 3200 cm^{-1} was attributed to the stretching vibration of hydroxyl (–OH) groups, while the peak at 1638 cm^{-1} was assigned to the bending vibration of adsorbed water molecules [79]. The peaks observed at 2920 cm^{-1} and around 2851 cm^{-1} were attributed to the stretching vibrations of C–H [80]. The peaks at 1733, 1631, and 1438 cm^{-1} were assigned to the bending vibration of the C=O, C=C, and $–COO^-$ group, respectively, while the peak at 1379 cm^{-1} was attributed to the bending vibration of C-H bonds in ester group [80]. The peak observed around 1125 cm^{-1} was assigned to the stretching vibration of the Zn–O bond [78]. The presence of this peak confirms the formation of ZS-ZnO-NPs. The intensity of this peak varied depending on the type of zinc salt used, indicating the influence of the precursor on the bonding characteristics of the nanoparticles. In addition, the peaks between 680 and 400 cm^{-1} were attributed to the Zn-O bending vibration, which is also a characteristic peak of ZnO-NPs [20,65]. The $ZnCl_2$ resulted in the highest absorbance among the synthesized ZS-ZnO-NPs, followed by $ZnSO_4 \cdot H_2O$, $Zn(CH_3COO)_2 \cdot 2H_2O$, and $Zn(NO_3)_2 \cdot 6H_2O$, as shown in Figure 8. The observed increase in absorbance could potentially be attributed to the smaller size of the nanoparticles. The observed trends indicate that there is a correlation between smaller particle sizes and a rise in absorbance and band area [78]. Finally, the FTIR spectra confirmed the presence of various functional groups on the surface of the synthesized ZS-ZnO-NPs, and the observed peaks were assigned to various functional groups based on the literature. The differences in the peak intensities and positions in the FTIR spectra of the synthesized ZS-ZnO-NPs were attributed to the use of different zinc salts, which influenced the bonding characteristics of the nanoparticles.

3.7. UV-Vis Spectroscopy

The UV-visible spectroscopy measurements provide information about the optical properties of green ZS-ZnO-NPs. ZnO-NPs have excellent UV absorption properties in the range of 200–400 nm, which make them suitable for various medical applications, such as

sunscreens and antiseptic ointments, as they can efficiently absorb and scatter UV radiation, providing effective skin protection against harmful UV rays [81]. The UV-visible spectrum of the absorbance of the ZS-ZnO-NPs is shown in Figure 9.

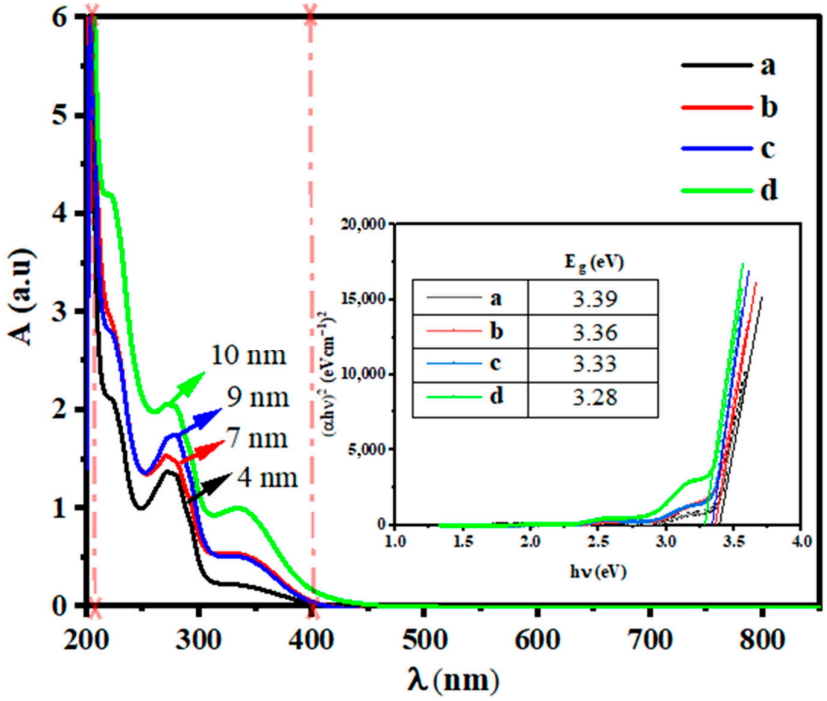

Figure 9. UV-visible spectrum of the absorbance and band gap energies (E_g, inside) of ZS-ZnO-NPs synthesized using different zinc salts and a plant extract of *Phoenix dactylifera* L. at pH 12: (a). $ZnCl_2$, (b). $ZnSO_4 \cdot H_2O$, (c). $Zn(CH_3COO)_2 \cdot 2H_2O$, and (d). $Zn(NO_3)_2 \cdot 6H_2O$.

The observed absorbances generally increased with an increase in nanoparticle size. Therefore, the trend of increasing UV-vis absorbance with increasing nanoparticle size observed in this study can be attributed to the larger size of the nanoparticles synthesized using $Zn(CH_3COO)_2 \cdot 2H_2O$ followed by those synthesized using $Zn(NO_3)_2 \cdot 6H_2O$, compared to those synthesized using $ZnSO_4 \cdot H_2O$ and $ZnCl_2$. Furthermore, the different zinc salts used in the synthesis process can also influence the optical properties of the nanoparticles, as the salts can affect the crystal structure, morphology, and surface properties of the ZS-ZnO-NPs (as shown by TEM and SEM), which can, in turn, affect their UV-visible absorbance properties. Similar studies have found that the absorption properties of nanoparticles can be affected by factors such as size, shape, and surface chemistry, as observed in biological triangular Au-NPs [82,83], TiO_2-NPs, and ZS-ZnO-NPs [84,85]. The gap energies of nanoparticles synthesized using different methods were determined and compared, revealing a trend of lower gap energies associated with larger nanoparticle sizes, suggesting that nanoparticle size may influence their optical and electronic properties. As shown in Figure 9 (Table), ZS-ZnO-NPs synthesized using $ZnCl_2$ exhibited the highest gap energy at 3.39 eV, followed by ZS-ZnO-NPs synthesized using $ZnSO_4 \cdot H_2O$ at 3.36 eV, and samples synthesized using both $Zn(CH_3COO)_2 \cdot 2H_2O$ as well as $Zn(NO_3)_2 \cdot 6H_2O$, showing slightly lower gap energies at 3.33 eV and 3.28 eV, respectively. This trend is attributed to the larger nanoparticle sizes (both D_{TEM} and D_{SEM}) being associated with lower gap energies. For instance, ZS-ZnO-NPs synthesized using $ZnCl_2$, which has the smallest D_{TEM} and D_{SEM} sizes, also exhibited the highest gap energy, while samples of ZS-ZnO-NPs synthesized using $Zn(CH_3COO)_2 \cdot 2H_2O$ and $Zn(NO_3)_2 \cdot 6H_2O$, which have larger D_{TEM} and D_{SEM} sizes, showed slightly lower gap energies. These findings suggest that nanoparticle size may play a role in influencing the electronic properties, with smaller nanoparticles potentially having higher gap energies.

3.8. Antioxidant Activity

The synthesized ZS-ZnO-NPs were evaluated for their antioxidant activity using the DPPH FR• assay. A series of experiments were performed with different concentrations (50–1000 µg/mL, Table 3) and incubation times (0.5–24 h, Table 3) to fully understand this property.

Table 3. Concentration-dependent (50, 125, 250, 500, and 1000 µg/mL) and time-dependent (0.5, 3, 6, 12, and 24 h) trends in antioxidant activity (IP% DPPH inhibition) of ZS-ZnO-NPs synthesized using different zinc salts and a plant extract of *Phoenix dactylifera* L. at pH 12: (a). $ZnCl_2$, (b). $ZnSO_4 \cdot H_2O$, (c). $Zn(CH_3COO)_2 \cdot 2H_2O$, and (d). $Zn(NO_3)_2 \cdot 6H_2O$.

IP (%)																				
Time (h)	**0.5**				**3**				**6**				**12**				**24**			
C (µg/mL)	**a**	**b**	**c**	**d**	**a**	**b**	**c**	**d**	**a**	**b**	**c**	**d**	**a**	**b**	**c**	**d**	**a**	**b**	**c**	**d**
50	33.9	37.2	35.8	26.1	41.2	47.9	42.8	36.4	48.2	56.4	49.5	43.7	56.7	68.3	59.3	52.3	64.8	79.1	68.6	64.9
125	47.7	50.6	48.5	34.2	56.9	63.7	59.6	47.6	64.6	71.6	67.8	54.9	70.6	80.1	74.8	65.7	93.2	94.3	95.2	72.3
250	61.4	62.4	59.8	45.8	73.2	75.1	69.8	59.1	78.6	82.5	75.8	68.1	85.8	88.2	82.5	78.5	97.5	99.1	98.8	90.5
500	73.1	74.3	69.7	57.3	78.5	79.2	75.6	70.8	85.2	86.2	81.2	79.5	90.8	91.3	86.9	85.6	98.4	99.7	99.2	94.6
1000	77.5	78.3	73.9	68.5	81.7	83.1	78.6	76.9	88.1	88.9	84.6	84.6	92.7	93.2	89.3	89.2	99.1	99.8	99.3	97.4

Note: Rows with the same values in the time column for a given concentration indicate no significant difference in antioxidant activity (IP% DPPH inhibition) between the corresponding time points.

The results, as shown in Figure 10 (Table 3), demonstrated that all ZS-ZnO-NPs exhibited antioxidant activity, and there was an increase in antioxidant activity with increasing concentration and incubation time.

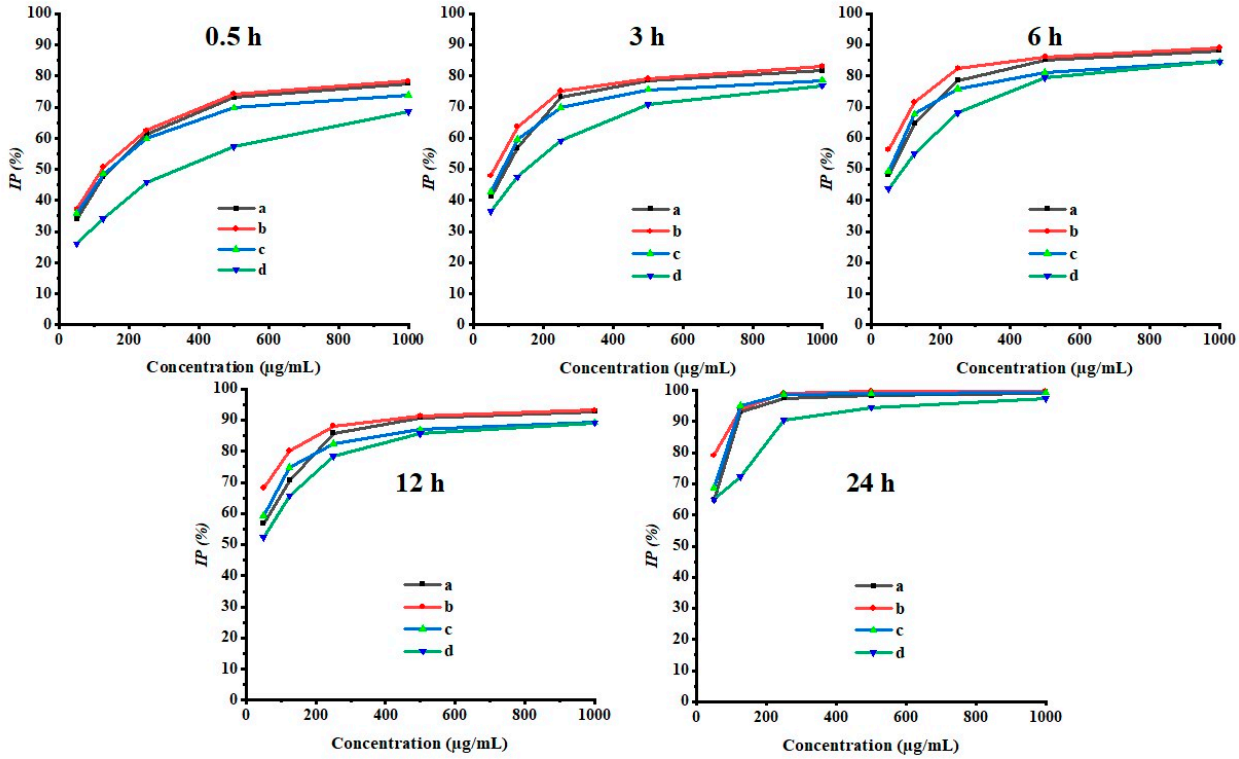

Figure 10. Concentration-dependent (50, 125, 250, 500, and 1000 µg/mL) and time-dependent (0.5, 3, 6, 12, and 24 h) trends in antioxidant activity (*IP* % DPPH inhibition) of ZS-ZnO-NPs synthesized using different zinc salts and a plant extract of *Phoenix dactylifera* L. at pH 12: (a). $ZnCl_2$, (b). $ZnSO_4 \cdot H_2O$, (c). $Zn(CH_3COO)_2 \cdot 2H_2O$, and (d). $Zn(NO_3)_2 \cdot 6H_2O$.

Specifically, ZS-ZnO-NPs synthesized using $ZnSO_4 \cdot H_2O$ exhibited the highest scavenging activity among all the tested concentrations and incubation times, with inhibition percentages ranging from 37.2% to 78.3% at 50–1000 µg/mL after 0.5 h of incubation. $ZnCl_2$ showed 77.5% inhibition at 1000 µg/mL after 0.5 h of incubation, followed by $Zn(CH_3COO)_2 \cdot 2H_2O$ with 73.9% inhibition at 1000 µg/mL after 0.5 h of incubation and $Zn(NO_3)_2 \cdot 6H2O$ with 68.5% inhibition. The antioxidant activity of the ZS-ZnO-NPs was found to be concentration-dependent, with higher concentrations resulting in higher antioxidant activity. This could be due to the increased availability of ZS-ZnO-NPs to scavenge free radicals at higher concentrations. Moreover, the antioxidant activity of ZS-ZnO-NPs also increased with increasing the concentration and incubation time up to a certain point, beyond which the activity plateaued. For example, at 500 µg/mL of ZS-ZnO-NPs synthesized using $ZnSO_4 \cdot H_2O$, the antioxidant activity was 91.3% after 12 h of incubation but increased to 93.2% at 1000 µg/mL after the same time of incubation. These findings suggest that the antioxidant activity of ZS-ZnO-NPs is concentration- and time-dependent and can be modulated by varying these parameters. The observed differences in antioxidant activity among different zinc salts used in the synthesis, such as $ZnSO_4 \cdot H_2O$, $ZnCl_2$, $Zn(CH_3COO)_2 \cdot 2H_2O$, as well as $Zn(NO_3)_2 \cdot 6H_2O$, could be attributed to their varying chemical properties. For example, $ZnSO_4 \cdot H_2O$ has been reported to have higher antioxidant activity compared to other zinc salts, and this property may have been transferred to the synthesized ZS-ZnO-NPs [86]. Furthermore, the stabilizing agents inherent in the *Phoenix* extract utilized during the synthesis might play a role in the discerned variations in antioxidant activity. The phytochemicals within the extract may possess functional groups capable of interacting with reactive oxygen species (ROS), such as superoxide anion (O^{2-}), hydrogen peroxide (H_2O_2), and hydroxyl radical ($OH^{\cdot}$). These ROS can engage with functional proteins through both specific and non-specific binding mechanisms on the surface of the nanoparticles. This intricate interaction potentially contributes to an augmented antioxidant activity [87–90]. Additionally, another possible justification for this observation could be the unique morphology of ZnO nanoparticles synthesized from $ZnSO_4 \cdot H_2O$, which were reported to exhibit hollow spherical, nanorings, and spheroidal morphology (See Section 3.4). These morphological characteristics could provide a larger surface area for interaction with free radicals, leading to enhanced antioxidant activity. Moreover, the size and morphology of the green-synthesized ZS-ZnO-NPs could also play a role in their antioxidant activity, with smaller nanoparticles generally exhibiting higher antioxidant activity due to their increased surface area and reactivity. Therefore, the smaller particle size of $ZnCl_2$-synthesized ZS-ZnO-NPs compared to the other salts could have contributed to their relatively higher antioxidant activity [91,92].

Furthermore, the incubation time of the nanoparticles with the DPPH radical may also play a role in their antioxidant activity. Longer incubation times could allow for more efficient scavenging of free radicals by ZS-ZnO-NPs, leading to higher antioxidant activity.

The concentration-dependent and time-dependent trends in antioxidant activity observed in this study are consistent with previous reports on the antioxidant properties of ZS-ZnO-NPs [93–95]. The results suggest that the synthesized ZS-ZnO-NPs exhibit concentration- and time-dependent antioxidant activity, and this property can be modulated by varying the concentration of ZS-ZnO-NPs and the incubation time.

It is worth mentioning that the antioxidant activity of nanoparticles is a complex phenomenon influenced by various factors, including their size, shape, surface chemistry, and stabilizing agents used in the synthesis. The differences in the chemical properties and solubility of the zinc salts used in the synthesis, such as $ZnCl_2$, $ZnSO_4 \cdot H_2O$, $Zn(CH_3COO)_2 \cdot 2H_2O$, as well as $Zn(NO_3)_2 \cdot 6H_2O$, have resulted in variations in the size, morphology, and surface chemistry of the synthesized ZS-ZnO-NPs, which in turn have influenced their antioxidant activity.

4. Conclusions

In summary, this study presents an efficient and sustainable synthesis of zinc salt-dependent zinc oxide nanoparticles (ZS-ZnO-NPs) utilizing diverse zinc salts ($ZnCl_2$, $ZnSO_4 \cdot H_2O$, $Zn(CH_3COO)_2 \cdot 2H_2O$, and $Zn(NO_3)_2 \cdot 6H_2O$) and plant extracts from *Phoenix dactylifera* L. The comprehensive evaluation covered the morphology, optical properties, stability, and antioxidant activity of the nanoparticles. Zeta potential measurements, SEM, TEM, XRD, UV-Vis spectroscopy, and FTIR analyses collectively confirmed the crystalline nature, size distribution, and chemical groups on the nanoparticle surface.

The comprehensive analysis of the synthesized ZS-ZnO-NPs revealed significant variations influenced by the choice of zinc salt. The nanoparticles exhibited sizes ranging from 3.7 to 10.2 nm, showcasing a clear size trend ($ZnCl_2 < ZnSO_4 \cdot H_2O < Zn(CH_3COO)_2 \cdot 2H_2O < Zn(NO_3)_2 \cdot 6H_2O$). The zeta potential trend ($ZnSO_4 \cdot H_2O < Zn(CH_3COO)_2 \cdot 2H_2O < Zn(NO_3)_2.6H_2O < ZnCl_2$) further emphasizes the impact of the zinc salt on surface charge. The XRD results indicated distinct crystalline properties, with a notable trend ($ZnCl_2 < ZnSO_4 \cdot H_2O < Zn(CH_3COO)_2 \cdot 2H_2O < Zn(NO_3)_2 \cdot 6H_2O$) in average crystallite size and corresponding trends in FWHM and crystallinity ($ZnCl_2 > ZnSO_4 \cdot H_2O > Zn(CH_3COO)_2 \cdot 2H_2O > Zn(NO_3)_2.6H_2O$). These trends highlight the critical role of the selected zinc salt in shaping the yield, stability, and structural characteristics of the nanoparticles. Correlating these findings, a clear relationship emerged between the choice of zinc salt and both nanoparticle size and crystalline structure. Notably, $ZnCl_2$ exhibited the smallest size and the highest crystallinity, aligning with its specific zinc salt properties. Moreover, the observed concentration and time-dependent inhibitory activity against DPPH free radicals further accentuates the potential applications of these nanoparticles across various industries. This study offers valuable insights into tailoring ZS-ZnO-NPs for diverse applications, including nutraceuticals, pharmaceuticals, cosmetics, biofuels, and environmental sectors. Further research under physiological conditions will provide additional support for potential biomedical and medical applications.

This study underscores the significance of merging biochemistry and engineering tools for efficient bioprocesses. It sheds light on the critical role of the chosen zinc salt in green synthesis, offering insights into various potential applications such as environmental remediation, (opto)electronics, nanomedicine, sensors, energy, detectors, green energy, and biotechnology. While contributing substantially to the synthesis and characterization of zinc oxide nanoparticles, ongoing research is imperative to address challenges and expand practical implications. The technology-driven green methods introduced here hold broad relevance across industries, necessitating further research to assess toxicity and broaden the scope of this work.

As we explore the multifaceted realm of ZnO-NPs, produced through the green synthesis method utilizing *Phoenix dactylifera* L. polyphenols with varied salt compositions, focusing on the anion effect, it is vital to assess their properties without the presence of the *Phoenix* polyphenol extract. This evaluation is crucial for a deeper understanding in future research, steering clear of reliance on chemically synthesized ZnO-NPs. To grasp the distinctions fully, future studies should meticulously scrutinize the structural and antioxidant characteristics of ZnO-NPs synthesized without the extract, potentially advancing their overall properties. This approach ensures a comprehensive comparison, underscoring the importance of further exploration to fully elucidate the distinctive aspects of both green synthesis and other methods. In conclusion, this study marks a significant step in advancing the synthesis and understanding of zinc oxide nanoparticles, emphasizing the continual need for exploration and refinement in this field.

Author Contributions: Conceptualization, J.A.A.A., A.G. and A.R.; methodology, J.A.A.A., A.G. and A.R.; software, J.A.A.A., A.G. and A.R.; validation, J.A.A.A., A.G. and A.R.; formal analysis, J.A.A.A., A.G. and A.R.; investigation, J.A.A.A., A.G. and A.R.; resources, J.A.A.A., A.G. and A.R.; data curation, J.A.A.A., A.G. and A.R.; writing—original draft preparation, J.A.A.A., A.G. and A.R.; writing—review and editing, J.A.A.A., A.G. and A.R.; visualization, J.A.A.A., A.G. and A.R.; supervision, J.A.A.A., A.G. and A.R.; project administration, J.A.A.A., A.G. and A.R.; funding acquisition, J.A.A.A., A.G. and A.R. All authors have read and agreed to the published version of the manuscript.

Funding: This research was funded by El Ministerio de Ciencia e Innovación, Agencia Estatal de Investigación, and Fondo Europeo de Desarrollo Regional (MCI/AEI/FEDER, UE) under project (Ref. PID2021-124294OB-C21).

Institutional Review Board Statement: Not applicable.

Informed Consent Statement: Not applicable.

Data Availability Statement: The data generated in this study are included in this article.

Acknowledgments: The authors acknowledge MCI/AEI/FEDER, UE that supports this work. In addition, the authors thank the predoctoral grant from Johar Amin Ahmed Abdullah (COOPERACIÓN al DESARROLLO de Universidad de Sevilla (CODE 810)). J.A.A.A. is thankful for the support from the Hayel Saeed Anam group represented by Abdul Jabbar Hayel Saeed Anam. The authors also thank El Centro de Investigación, Tecnología e Innovación (CITIUS) for granting access to area characterization and their assistance with the SEM, TEM, DRX, FTIR, and microscopy services.

Conflicts of Interest: The authors declare no conflicts of interest.

References

1. Umadevi, M.; Bindhu, M.R.; Sathe, V. A Novel Synthesis of Malic Acid Capped Silver Nanoparticles using Solanum lycopersicums Fruit Extract. *J. Mater. Sci. Technol.* **2013**, *29*, 317–322. [CrossRef]
2. Paul, D.R.; Robeson, L.M. Polymer nanotechnology: Nanocomposites. *Polymer* **2008**, *49*, 3187–3204. [CrossRef]
3. Jeevanandam, J.; Barhoum, A.; Chan, Y.S.; Dufresne, A.; Danquah, M.K. Review on nanoparticles and nanostructured materials: History, sources, toxicity and regulations. *Beilstein J. Nanotechnol.* **2018**, *9*, 1050–1074. [CrossRef]
4. Abdullah, J.A.A.; Díaz-García, Á.; Law, J.Y.; Romero, A.; Franco, V.; Guerrero, A. Quantifying the Structure and Properties of Nanomagnetic Iron Oxide Particles for Enhanced Functionality through Chemical Synthesis. *Nanomaterials* **2023**, *13*, 2242. [CrossRef] [PubMed]
5. Al-Maamori, M.H. Preparation and Surface Modification of Zinc Oxide Nanoparticles. *J. Babylon Univ. J. Appl. Pure Sci.* **2017**, *25*, 497–503.
6. Kolodziejczak-Radzimska, A.; Jesionowski, T. Zinc oxide-from synthesis to application: A review. *Materials* **2014**, *7*, 2833–2881. [CrossRef] [PubMed]
7. Wahab, R.; Hwang, I.H.; Shin, H.-S.; Kim, Y.-S.; Musarrat, J.; Al-Khedhairy, A.A.; Siddiqui, M.A. Zinc Oxide Nanostructures and their Applications. In *Intelligent Nanomaterials*; John Wiley & Sons, Inc.: Hoboken, NJ, USA, 2012; pp. 183–212, ISBN 9780470938799.
8. Mirzaei, H.; Darroudi, M. Zinc oxide nanoparticles: Biological synthesis and biomedical applications. *Ceram. Int.* **2017**, *43*, 907–914. [CrossRef]
9. Fahmy, M.D.; Jazayeri, H.E.; Razavi, M.; Hashemi, M.; Omidi, M.; Farahani, M.; Salahinejad, E.; Yadegari, A.; Pitcher, S.; Tayebi, L. Biomedical Applications of Intelligent Nanomaterials. *Intell. Nanomater. Second Ed.* **2016**, *13*, 199–245. [CrossRef]
10. Ashajyothi, C.; Harish, K.H.; Dubey, N.; Chandrakanth, R.K. Antibiofilm activity of biogenic copper and zinc oxide nanoparticles-antimicrobials collegiate against multiple drug resistant bacteria: A nanoscale approach. *J. Nanostruct. Chem.* **2016**, *6*, 329–341. [CrossRef]
11. Al-Mohaimeed, A.M.; Al-Onazi, W.A.; El-Tohamy, M.F. Multifunctional Eco-Friendly Synthesis of ZnO Nanoparticles in Biomedical Applications. *Molecules* **2022**, *27*, 579. [CrossRef]
12. Moezzi, A.; McDonagh, A.M.; Cortie, M.B. Zinc oxide particles: Synthesis, properties and applications. *Chem. Eng. J.* **2012**, *185–186*, 1–22. [CrossRef]
13. Singh, A.; Singh, N.B.; Hussain, I.; Singh, H.; Yadav, V.; Singh, S.C. Green synthesis of nano zinc oxide and evaluation of its impact on germination and metabolic activity of Solanum lycopersicum. *J. Biotechnol.* **2016**, *233*, 84–94. [CrossRef] [PubMed]
14. Markova, Z.; Novak, P.; Kaslik, J.; Plachtova, P.; Brazdova, M.; Jancula, D.; Siskova, K.M.; Machala, L.; Marsalek, B.; Zboril, R.; et al. Iron(II,III)-polyphenol complex nanoparticles derived from green tea with remarkable ecotoxicological impact. *ACS Sustain. Chem. Eng.* **2014**, *2*, 1674–1680. [CrossRef]
15. Nakbanpote, W.; Ruttanakorn, M.; Sukadeetad, K.; Sakkayawong, N.; Damrianant, S. Effects of drying and extraction methods on phenolic compounds and in vitro assays of *Eclipta prostrata* Linn leaf extracts. *ScienceAsia* **2019**, *45*, 127–137. [CrossRef]

16. Karam, M.C.; Petit, J.; Zimmer, D.; Baudelaire Djantou, E.; Scher, J. Effects of drying and grinding in production of fruit and vegetable powders: A review. *J. Food Eng.* **2016**, *188*, 32–49. [CrossRef]
17. Wu, J.; Chen, S.; Ge, S.; Miao, J.; Li, J.; Zhang, Q. Preparation, properties and antioxidant activity of an active film from silver carp (*Hypophthalmichthys molitrix*) skin gelatin incorporated with green tea extract. *Food Hydrocoll.* **2013**, *32*, 42–51. [CrossRef]
18. Toropov, N.; Vartanyan, T. Noble Metal Nanoparticles: Synthesis and Optical Properties. In *Comprehensive Nanoscience and Nanotechnology*; Elsevier: Amsterdam, The Netherlands, 2019; pp. 61–88, ISBN 9780128122969.
19. Zayed, M.F.; Eisa, W.H. *Phoenix dactylifera* L. leaf extract phytosynthesized gold nanoparticles; controlled synthesis and catalytic activity. *Spectrochim. Acta Part A Mol. Biomol. Spectrosc.* **2014**, *121*, 238–244. [CrossRef] [PubMed]
20. Mohammadi, F.M.; Ghasemi, N. Influence of temperature and concentration on biosynthesis and characterization of zinc oxide nanoparticles using cherry extract. *J. Nanostructure Chem.* **2018**, *8*, 93–102. [CrossRef]
21. Ghodake, G.S.; Deshpande, N.G.; Lee, Y.P.; Jin, E.S. Pear fruit extract-assisted room-temperature biosynthesis of gold nanoplates. *Colloids Surf. B Biointerfaces* **2010**, *75*, 584–589. [CrossRef]
22. Gajanan, G.; Chang, M.; Kim, J.; Jin, E. Biogenic materialization using pear extract intended for the synthesis and design of ordered gold nanostructures. *J. Mater. Sci.* **2011**, *46*, 4741–4747. [CrossRef]
23. Rodríguez-Carvajal, J. Recent advances in magnetic structure determination by neutron powder diffraction. *Phys. B Condens. Matter* **1993**, *192*, 55–69. [CrossRef]
24. Tran, N.; Mir, A.; Mallik, D.; Sinha, A.; Nayar, S.; Webster, T.J. Bactericidal effect of iron oxide nanoparticles on *Staphylococcus aureus*. *Int. J. Nanomed.* **2010**, *5*, 277–283. [CrossRef]
25. Baazaoui, N.; Sghaier-Hammami, B. Green Synthesis of Nanoparticles from Date Palm (*Phoenix dactylifera* L.). In *The Date Palm Genome, Vol. 2: Omics and Molecular Breeding*; Al-Khayri, J.M., Jain, S.M., Johnson, D.V., Eds.; Springer International Publishing: Cham, Switzerland, 2021; pp. 51–69, ISBN 9783030737504.
26. Abdullah, J.A.A.; Salah Eddine, L.; Abderrhmane, B.; Alonso-González, M.; Guerrero, A.; Romero, A. Green synthesis and characterization of iron oxide nanoparticles by pheonix dactylifera leaf extract and evaluation of their antioxidant activity. *Sustain. Chem. Pharm.* **2020**, *17*, 100280. [CrossRef]
27. Eddine, L.S.; Segni, L.; Noureddine, G.; Redha, O.M.; Sonia, M. Scavenging Activity, Anti-Inflammatory and Diabetes Related Enzyme Inhibition Properties of Leaves Extract from some Varieties of *Phoenyx dactylifera* L. *Int. Lett. Chem. Phys. Astron.* **2013**, *14*, 125–135. [CrossRef]
28. Mohamed, A.; Shafey, E. Green synthesis of metal and metal oxide nanoparticles from plant leaf extracts and their applications: A review. *Green Process. Synth.* **2020**, *9*, 304–339. [CrossRef]
29. Jayachandran, A.; Aswathy, T.R.; Nair, A.S. Green synthesis and characterization of zinc oxide nanoparticles using *Cayratia pedata* leaf extract. *Biochem. Biophys. Rep.* **2021**, *26*, 100995. [CrossRef]
30. Kim, S.-K.; Ngo, D.-H.; Vo, T.-S. Marine Fish-Derived Bioactive Peptides as Potential Antihypertensive Agents. *Adv. Food Nutr. Res.* **2012**, *65*, 249–260. [PubMed]
31. Gudipati, V. Fish Gelatin: A Versatile Ingredient for the Food and Pharmaceutical Industries. In *Marine Proteins and Peptides*; John Wiley & Sons, Ltd.: Chichester, UK, 2013; pp. 271–295.
32. Rawdkuen, S.; Thitipramote, N.; Benjakul, S. Preparation and functional characterisation of fish skin gelatin and comparison with commercial gelatin. *Int. J. Food Sci. Technol.* **2013**, *48*, 1093–1102. [CrossRef]
33. Etxabide, A.; Uranga, J.; Guerrero, P.; de la Caba, K. Development of active gelatin films by means of valorisation of food processing waste: A review. *Food Hydrocoll.* **2017**, *68*, 192–198. [CrossRef]
34. Nwakaudu, A.A.; Nwakaudu, M.S.; Owuamanam, C.I.; Iheaturu, N.C. The Use of Natural Antioxidant Active Polymer Packaging Films for Food Preservation. *Appl. Signals Rep.* **2015**, *2*, 38–50.
35. Jeevithan, E.; Qingbo, Z.; Bao, B.; Wu, W. Biomedical and Pharmaceutical Application of Fish Collagen and Gelatin: A Review. *J. Nutr. Ther.* **2013**, *2*, 218–227. [CrossRef]
36. Liu, L.S.; Liu, C.K.; Fishman, M.L.; Hicks, K.B. Composite films from pectin and fish skin gelatin or soybean flour protein. *J. Agric. Food Chem.* **2007**, *55*, 2349–2355. [CrossRef]
37. Abdullah, J.A.A.; Rosado, M.J.; Guerrero, A.; Romero, A. Eco-friendly synthesis of ZnO-nanoparticles using *Phoenix dactylifera* L., polyphenols: Physicochemical, microstructural, and functional assessment. *New J. Chem.* **2023**, *47*, 4409–4417. [CrossRef]
38. Abdullah, J.A.A.; Yemişken, E.; Guerrero, A.; Romero, A. Marine Collagen-Based Antibacterial Film Reinforced with Graphene and Iron Oxide Nanoparticles. *Int. J. Mol. Sci.* **2022**, *24*, 648. [CrossRef] [PubMed]
39. Dulta, K.; Koşarsoy Ağçeli, G.; Chauhan, P.; Jasrotia, R.; Chauhan, P.K.; Ighalo, J.O. Multifunctional CuO nanoparticles with enhanced photocatalytic dye degradation and antibacterial activity. *Sustain. Environ. Res.* **2022**, *32*, 2. [CrossRef]
40. Abdullah, J.A.A.; Díaz-García, Á.; Law, J.Y.; Romero, A.; Franco, V.; Guerrero, A. Sustainable Nanomagnetism: Investigating the Influence of Green Synthesis and pH on Iron Oxide Nanoparticles for Enhanced Biomedical Applications. *Polymers* **2023**, *15*, 3850. [CrossRef]
41. Abdullah, J.A.A.; Jiménez-Rosado, M.; Guerrero, A.; Romero, A. Effect of Calcination Temperature and Time on the Synthesis of Iron Oxide Nanoparticles: Green vs. Chemical Method. *Materials* **2023**, *16*, 1798. [CrossRef]
42. Abdullah, J.A.A.; Jiménez-Rosado, M.; Guerrero, A.; Romero, A. Biopolymer-Based Films Reinforced with Green Synthesized Zinc Oxide Nanoparticles. *Polymers* **2022**, *14*, 5202. [CrossRef]

43. Bibi, I.; Kamal, S.; Ahmed, A.; Iqbal, M.; Nouren, S.; Jilani, K.; Nazar, N.; Amir, M.; Abbas, A.; Ata, S.; et al. Nickel nanoparticle synthesis using *Camellia sinensis* as reducing and capping agent: Growth mechanism and photo-catalytic activity evaluation. *Int. J. Biol. Macromol.* **2017**, *103*, 783–790. [CrossRef]
44. Abdullah, J.A.A.; Benítez, J.J.; Guerrero, A.; Romero, A. Sustainable Integration of Zinc Oxide Nanoparticles: Enhancing Properties of Poly (ε-Caprolactone) Electrospun Nanofibers and Cast Films. *Coatings* **2023**, *13*, 1665. [CrossRef]
45. Barzinjy, A.A.; Azeez, H.H. Green synthesis and characterization of zinc oxide nanoparticles using *Eucalyptus globulus* Labill. leaf extract and zinc nitrate hexahydrate salt. *SN Appl. Sci.* **2020**, *2*, 991. [CrossRef]
46. Ayachi, A.A.; Mechakra, H.; Silvan, M.M.; Boudjaadar, S.; Achour, S. Monodisperse α-Fe_2O_3 nanoplatelets: Synthesis and characterization. *Ceram. Int.* **2015**, *41*, 2228–2233. [CrossRef]
47. Mallick, P.; Dash, B.N. X-ray Diffraction and UV-Visible Characterizations of α-Fe_2O_3 Nanoparticles Annealed at Different Temperature. *Nanosci. Nanotechnol.* **2013**, *3*, 130–134.
48. Wilcox, R.J.; Losey, B.P.; Folmer, J.C.W.; Martin, J.D.; Zeller, M.; Sommer, R. Crystalline and liquid structure of zinc chloride trihydrate: A unique ionic liquid. *Inorg. Chem.* **2015**, *54*, 1109–1119. [CrossRef] [PubMed]
49. National Center for Biotechnology Information. PubChem Compound Summary for CID 11192, Zinc Acetate. In *Kirk-Othmer Encyclopedia of Chemical Technology*, 4th ed.; John Wiley Sons: New York, NY, USA, 2023; Volume 1, p. V25 841.
50. Saha, J.; Podder, J. Crystallization of Zinc Sulphate Single Crystals and Its Structural, Thermal and Optical Characterization. *J. Bangladesh Acad. Sci.* **1970**, *35*, 203–210. [CrossRef]
51. Reid, B.T.; Reed, S.M. Improved methods for evaluating the environmental impact of nanoparticle synthesis. *Green Chem.* **2016**, *18*, 4263–4269. [CrossRef] [PubMed]
52. Serrano-Lotina, A.; Portela, R.; Baeza, P.; Alcolea-Rodriguez, V.; Villarroel, M.; Ávila, P. Zeta potential as a tool for functional materials development. *Catal. Today* **2022**, *423*, 113862. [CrossRef]
53. Shokry Hassan, H.; Kashyout, A.B.; Soliman, H.M.A.; Uosif, M.A.; Afify, N. Influence of Reaction Time, Reducing Agent and Zinc Precursors on the Morphological Structures of Zinc Oxide. *Angl. J.* **2013**, *3*.
54. Rukhadze, M.; Wotocek, M.; Kuhn, S.; Hempelmann, R. Influence of Anions of the Hofmeister Series on the Size of ZnS Nanoparticles Synthesised via Reverse Microemulsion Systems. In *UK Colloids 2011: An International Colloid and Surface Science Symposium*; Springer: Berlin/Heidelberg, Germany, 2012; pp. 67–72. [CrossRef]
55. Gregory, K.P.; Elliott, G.R.; Robertson, H.; Kumar, A.; Wanless, E.J.; Webber, G.B.; Craig, V.S.J.; Andersson, G.G.; Page, A.J. Understanding specific ion effects and the Hofmeister series. *Phys. Chem. Chem. Phys.* **2022**, *24*, 12682–12718. [CrossRef] [PubMed]
56. Fuad, A.; Fibriyanti, A.A.; Subakti; Mufti, N.; Taufiq, A. Effect of Precursor Concentration Ratio on The Crystal Structure, Morphology, and Band Gap of ZnO Nanorods. *IOP Conf. Ser. Mater. Sci. Eng.* **2017**, *202*, 012074. [CrossRef]
57. Park, J.H.; Park, C.; Lee, K.S.; Suh, S.J. Effect of NaOH and precursor concentration on size and magnetic properties of FeCo nanoparticles synthesized using the polyol method. *AIP Adv.* **2020**, *10*, 115220. [CrossRef]
58. Andarini, N.; Farida, R.S.; Haryati, T. The Effect of Different Precursor Concentration on The Synthesis of CaO Nanoparticles with Coprecipitation Methods for Palm Oil Transesterification Catalysis. *Reaktor* **2021**, *21*, 45–51. [CrossRef]
59. Sibiya, P.N.; Moloto, M.J. Effect of precursor concentration and pH on the shape and size of starch capped silver selenide (Ag_2Se) nanoparticles. *Chalcogenide Lett.* **2014**, *11*, 577–588.
60. Wang, H.; Han, X.; Chen, Y.; Guo, W.; Zheng, W.; Cai, N.; Guo, Q.; Zhao, X.; Wu, F. Effects of F^-, Cl^-, Br^-, $NO_3{}^-$, and $SO_4{}^{2-}$ on the colloidal stability of Fe_3O_4 nanoparticles in the aqueous phase. *Sci. Total Environ.* **2021**, *757*, 143962. [CrossRef] [PubMed]
61. Sundarabharathi, L.; Ponnamma, D.; Parangusan, H.; Chinnaswamy, M.; Al-Maadeed, M.A.A. Effect of anions on the structural, morphological and dielectric properties of hydrothermally synthesized hydroxyapatite nanoparticles. *SN Appl. Sci.* **2020**, *2*, 94. [CrossRef]
62. Suresh, R.; Ponnuswamy, V.; Sankar, C.; Manickam, M.; Venkatesan, S.; Perumal, S. NiO nanoflakes: Effect of anions on the structural, optical, morphological and magnetic properties. *J. Magn. Magn. Mater.* **2017**, *441*, 787–794. [CrossRef]
63. Kim, H.S.; Seo, Y.S.; Kim, K.; Han, J.W.; Park, Y.; Cho, S. Concentration Effect of Reducing Agents on Green Synthesis of Gold Nanoparticles: Size, Morphology, and Growth Mechanism. *Nanoscale Res. Lett.* **2016**, *11*, 230. [CrossRef]
64. Pudukudy, M.; Yaakob, Z. Facile Synthesis of Quasi Spherical ZnO Nanoparticles with Excellent Photocatalytic Activity. *J. Clust. Sci.* **2015**, *26*, 1187–1201. [CrossRef]
65. Soto-Robles, C.A.; Luque, P.A.; Gómez-Gutiérrez, C.M.; Nava, O.; Vilchis-Nestor, A.R.; Lugo-Medina, E.; Ranjithkumar, R.; Castro-Beltrán, A. Study on the effect of the concentration of Hibiscus sabdariffa extract on the green synthesis of ZnO nanoparticles. *Results Phys.* **2019**, *15*, 102807. [CrossRef]
66. Liu, X.; Ye, L.; Liu, S.; Li, Y.; Ji, X. Photocatalytic reduction of CO_2 by ZnO micro/nanomaterials with different morphologies and ratios of {0001} facets. *Sci. Rep.* **2016**, *6*, 38474. [CrossRef]
67. Tuoriniemi, J.; Johnsson, A.C.J.H.; Holmberg, J.P.; Gustafsson, S.; Gallego-Urrea, J.A.; Olsson, E.; Pettersson, J.B.C.; Hassellöv, M. Intermethod comparison of the particle size distributions of colloidal silica nanoparticles. *Sci. Technol. Adv. Mater.* **2014**, *15*, 35009. [CrossRef] [PubMed]
68. Albertsson, J.; Abrahams, S.C.; Kvick, Å. Atomic displacement, anharmonic thermal vibration, expansivity and pyroelectric coefficient thermal dependences in ZnO. *Acta Crystallogr. Sect. B Struct. Sci.* **1989**, *45*, 34–40. [CrossRef]

69. Suresh, D.; Nethravathi, P.C.; Udayabhanu; Pavan Kumar, M.A.; Raja Naika, H.; Nagabhushana, H.; Sharma, S.C. Chironji mediated facile green synthesis of ZnO nanoparticles and their photoluminescence, photodegradative, antimicrobial and antioxidant activities. *Mater. Sci. Semicond. Process.* **2015**, *40*, 759–765. [CrossRef]
70. Wang, X.; Yang, D.P.; Huang, P.; Li, M.; Li, C.; Chen, D.; Cui, D. Hierarchically assembled Au microspheres and sea urchin-like architectures: Formation mechanism and SERS study. *Nanoscale* **2012**, *4*, 7766–7772. [CrossRef]
71. Pelicano, C.M.; Yanagi, H. Effect of rubrene: P3HT bilayer on photovoltaic performance of perovskite solar cells with electrodeposited ZnO nanorods. *J. Energy Chem.* **2018**, *27*, 455–462. [CrossRef]
72. Pelicano, C.M.; Yanagi, H. Efficient solid-state perovskite solar cells based on nanostructured zinc oxide designed by strategic low temperature water oxidation. *J. Mater. Chem. C* **2017**, *5*, 8059–8070. [CrossRef]
73. Singh, J.; Dutta, T.; Kim, K.-H.; Rawat, M.; Samddar, P.; Kumar, P. 'Green' synthesis of metals and their oxide nanoparticles: Applications for environmental remediation. *J. Nanobiotechnol.* **2018**, *16*, 84. [CrossRef]
74. Mukunthan, K.S.; Balaji, S. Cashew Apple Juice (*Anacardium occidentale* L.) Speeds Up the Synthesis of Silver Nanoparticles. *Int. J. Green Nanotechnol.* **2012**, *4*, 71–79. [CrossRef]
75. Love, A.J.; Makarov, V.V.; Sinitsyna, O.V.; Shaw, J.; Yaminsky, I.V.; Kalinina, N.O.; Taliansky, M.E. A Genetically Modified Tobacco Mosaic Virus that can Produce Gold Nanoparticles from a Metal Salt Precursor. *Front. Plant Sci.* **2015**, *6*, 984. [CrossRef] [PubMed]
76. Vega-Poot, A.G.; Rodríguez-Gattorno, G.; Soberanis-Domínguez, O.E.; Patiño-Díaz, R.T.; Espinosa-Pesqueira, M.; Oskam, G. The nucleation kinetics of ZnO nanoparticles from $ZnCl_2$ in ethanol solutions. *Nanoscale* **2010**, *2*, 2710–2717. [CrossRef]
77. Hosseini Largani, S.; Akbarzadeh Pasha, M. The effect of concentration ratio and type of functional group on synthesis of CNT–ZnO hybrid nanomaterial by an in situ sol–gel process. *Int. Nano Lett.* **2017**, *7*, 25–33. [CrossRef]
78. Udvardi, B.; Kovács, I.J.; Fancsik, T.; Kónya, P.; Bátori, M.; Stercel, F.; Falus, G.; Szalai, Z. Effects of Particle Size on the Attenuated Total Reflection Spectrum of Minerals. *Appl. Spectrosc.* **2017**, *71*, 1157–1168. [CrossRef]
79. Mohan Kumar, K.; Mandal, B.K.; Siva Kumar, K.; Sreedhara Reddy, P.; Sreedhar, B. Biobased green method to synthesise palladium and iron nanoparticles using *Terminalia chebula* aqueous extract. *Spectrochim. Acta Part A Mol. Biomol. Spectrosc.* **2013**, *102*, 128–133. [CrossRef]
80. Salgado, P.; Márquez, K.; Rubilar, O.; Contreras, D.; Vidal, G. The effect of phenolic compounds on the green synthesis of iron nanoparticles (Fe_xO_y-NPs) with photocatalytic activity. *Appl. Nanosci.* **2019**, *9*, 371–385. [CrossRef]
81. AL-Asady, Z.M.; AL-Hamdani, A.H.; Hussein, M.A. Study the optical and morphology properties of zinc oxide nanoparticles. In Proceedings of the AIP Conference Proceedings of the 2nd International Conference on Materials Engineering & Science (IConMEAS 2019), Baghdad, Iraq, 25–29 September 2019; AIP Publishing: Melville, MA, USA, 2020; p. 020061.
82. Smitha, S.L.; Gopchandran, K.G.; Smijesh, N.; Philip, R. Size-dependent optical properties of Au nanorods. *Prog. Nat. Sci. Mater. Int.* **2013**, *23*, 36–43. [CrossRef]
83. Shankar, S.S.; Rai, A.; Ankamwar, B.; Singh, A.; Ahmad, A.; Sastry, M. Biological synthesis of triangular gold nanoprisms. *Nat. Mater.* **2004**, *3*, 482–488. [CrossRef] [PubMed]
84. Saikia, L.; Bhuyan, D.; Saikia, M.; Malakar, B.; Dutta, D.K.; Sengupta, P. Photocatalytic performance of ZnO nanomaterials for self sensitized degradation of malachite green dye under solar light. *Appl. Catal. A Gen.* **2015**, *490*, 42–49. [CrossRef]
85. Goh, E.G.; Xu, X.; McCormick, P.G. Effect of particle size on the UV absorbance of zinc oxide nanoparticles. *Scr. Mater.* **2014**, *78–79*, 49–52. [CrossRef]
86. Ruiz-Torres, N.; Flores-Naveda, A.; Barriga-Castro, E.D.; Camposeco-Montejo, N.; Ramírez-Barrón, S.; Borrego-Escalante, F.; Niño-Medina, G.; Hernández-Juárez, A.; Garza-Alonso, C.; Rodríguez-Salinas, P.; et al. Zinc oxide nanoparticles and zinc sulfate impact physiological parameters and boosts lipid peroxidation in soil grown coriander plants (*Coriandrum sativum*). *Molecules* **2021**, *26*, 1988. [CrossRef] [PubMed]
87. Junaid, M.; Dowlath, H.; Anjum, S.; Khalith, S.B.M.; Varjani, S.; Kumar, S.; Munuswamy, G.; Woong, S.; Jin, W.; Ravindran, B. Comparison of characteristics and biocompatibility of green synthesized iron oxide nanoparticles with chemical synthesized nanoparticles. *Environ. Res.* **2021**, *201*, 111585. [CrossRef]
88. Demirbas, A.; Welt, B.A.; Ocsoy, I. Biosynthesis of red cabbage extract directed Ag NPs and their effect on the loss of antioxidant activity. *Mater. Lett.* **2016**, *179*, 20–23. [CrossRef]
89. Zhao, X.; Zhou, L.; Shahid, M.; Rajoka, R.; Yan, L.; Shao, D.; Zhu, J.; Shi, J.; Huang, Q.; Yang, H. Critical Reviews in Biotechnology Fungal silver nanoparticles: Synthesis, application and challenges. *Crit. Rev. Biotechnol.* **2018**, *38*, 817–835. [CrossRef]
90. Küp, F.Ö.; Çoşkunçay, S.; Duman, F. Biosynthesis of silver nanoparticles using leaf extract of Aesculus hippocastanum (*Horse chestnut*): Evaluation of their antibacterial, antioxidant and drug release system activities. *Mater. Sci. Eng. C* **2020**, *107*, 110207. [CrossRef] [PubMed]
91. Myint, K.Z.; Yu, Q.; Xia, Y.; Qing, J.; Zhu, S.; Fang, Y.; Shen, J. Bioavailability and antioxidant activity of nanotechnology-based botanic antioxidants. *J. Food Sci.* **2021**, *86*, 284–292. [CrossRef] [PubMed]
92. Keshari, A.K.; Srivastava, R.; Singh, P.; Yadav, V.B.; Nath, G. Antioxidant and antibacterial activity of silver nanoparticles synthesized by *Cestrum nocturnum*. *J. Ayurveda Integr. Med.* **2020**, *11*, 37–44. [CrossRef] [PubMed]
93. Rajakumar, G.; Thiruvengadam, M.; Mydhili, G.; Gomathi, T.; Chung, I.M. Green approach for synthesis of zinc oxide nanoparticles from *Andrographis paniculata* leaf extract and evaluation of their antioxidant, anti-diabetic, and anti-inflammatory activities. *Bioprocess Biosyst. Eng.* **2018**, *41*, 21–30. [CrossRef] [PubMed]

94. Safawo, T.; Sandeep, B.V.; Pola, S.; Tadesse, A. Synthesis and characterization of zinc oxide nanoparticles using tuber extract of anchote (*Coccinia abyssinica* (Lam.) Cong.) for antimicrobial and antioxidant activity assessment. *OpenNano* **2018**, *3*, 56–63. [CrossRef]
95. Abdullah, J.A.A.; Perez-Puyana, V.; Guerrero, A.; Romero, A. Novel hybrid electrospun poly (ε-caprolactone) nanofibers containing green and chemical magnetic iron oxide nanoparticles. *J. Appl. Polym. Sci.* **2023**, *140*, e54345. [CrossRef]